36

MATHEMATICAL MODELING AS A NEW APPROACH FOR IMPROVING THE EFFICACY/TOXICITY PROFILE OF DRUGS: THE THROMBOCYTOPENIA CASE STUDY

ZVIA AGUR[1,2], MORAN ELISHMERENI[1], YURI KOGAN[1], YURI KHEIFETZ[1], IRIT ZIV[2], MEIR SHOHAM[2], AND VLADIMIR VAINSTEIN[1,2]

[1]*Institute for Medical Biomathematics (IMBM), Israel*

[2]*Optimata Ltd., Israel*

Contents

Preclinical Development Handbook: ADME and Biopharmaceutical Properties,
Edited by Shane Cox Gad

36.1 Introduction

Despite recent innovations, many life-threatening diseases still lack effective treatments. In March 2004, the Food and Drug Administration (FDA) agency issued a major report that identifies both the problems and the potential solutions for bringing more breakthroughs in the medical science to patients, as quickly and efficiently as possible. The report looks at the development processes for drugs, biologics, and medical devices, and calls for a joint effort of industry, academic researchers, product developers, patient groups, and the FDA to identify key problems and to develop solutions: "… A new product development toolkit -- containing powerful new scientific and technical methods such as computer-based predictive models... is urgently needed to improve predictability and efficiency along the critical path from laboratory concept to commercial product." [24]. The role of the present chapter is to demonstrate how the science of biomathematics can be harnessed for improving the solution of safety issues in the critical path of drug development, in general, and in the transition from the preclinical phases to Phase I, in particular.

36.1.1 Biomathematics and its use for rationalizing drug treatment strategies: a short history

A new synthesis of ecology and 'hard' biology, called biomathematics, emerged in the second half of the 20th century in the scientific community. Its role was to rationalize complex biological processes. Thus, in contrast to experimental biologists, who work at the microscopic cellular level and develop analytic tools that are analogous to the stills camera in photography, biomathematicians develop formulae, which effectively animate these shots, allowing us to understand the dynamics of the complex process we are investigating. Biomathematics has enabled the development of a range of new theories dealing with significant problems of disease progression and control, hitherto beyond the reach of 'snap shot', experimental biology.

But in spite of these efforts, until recently the biomedical research community was unanimous in viewing biological systems as too complex to enable accurate retrieval by mathematical models. This declarable mistrust in the power of biomathematics left the biomedical sciences lagging behind other sciences, as an immature sequel of experimental observations. In recent years, the somewhat disillusioned post-genomic era has rediscovered biological complexity, renaming it “system biology”. It seems that, finally, biomathematicians are becoming legitimate and almost beloved children of the scientific community.

In the 1980’s, notions from population dynamics have been used by Agur and colleagues to develop relatively simple formulae describing the growth patterns of interwoven populations of healthy and cancerous cells, formulae which have resulted in new drug regimens where the toxicity of chemotherapy has been significantly reduced [2,3,63]. The power of mathematics here was to prove the universality of the theoretical results and, therefore, to justify and encourage collaboration with cancer research experimentalists. The latter not only verified the theory in the laboratory, but also pinpointed the feasibility and strength of the theory-to-lab arrow [4,5].

In the above mentioned mathematical models, populations are subjected to a loss process due to randomly occurring environmental disturbances, which are effective only during a portion of the life-cycle. The models are studied over a large range of time-scales of the environmental change and for different degrees of variance in the system parameters. Analysis shows that the expected survival time of the population has a strong non-monotonic dependence on the relation between the duration of the disturbance-resistant life-stages and the periodicity of the environmental disturbance. This effect, termed "resonance phenomenon", was found at integer and fractional multiple of this relation. Interestingly, persistence in all harshly-varying environments is shown to depend on the degree of resonance in the environmental and population processes [2,6-8,64].

The universality of the resonance phenomenon, and its implication that the frequency of environmental disturbances determines population growth, seemed to offer attractive possibilities for the control of the cancer disease. Thus, Agur and colleagues have shown, both theoretically and experimentally, how the resonance phenomenon could be employed for choosing cytotoxic drug regimens that allow discrimination between different target cell populations. More specifically, it was asserted that one could determine the period of drug pulses, so as to maximize the elimination of malignant cells and, at the same time, to minimize the destruction of drug-susceptible host cells.

In the first stage, it was necessary to investigate the generality of the resonance phenomenon for the dynamics of different host cell populations. To allow analytical tractability and, hence, parameter-independent conclusions, deliberately crude mathematical models of the cancer patient were constructed, making simplified assumptions that both tumor and target host tissues are cells that vary only in cell-cycle parameters. The spatial arrangement of these cells was hence ignored. The interest was focused on comparing the overall behavior of the tumor to that of the host target tissues under different chemotherapy regimens of cell-cycle-phase-specific drugs, and on finding regimens that are selective to cancer cells. The conviction was that only a simplified model can clarify the underlying properties of the biomedical scenario. Model analysis showed that the resonance phenomenon is valid when considering drug-

induced myelotoxicity and tumor progression. Specifically, the mathematical analysis suggested that the efficacy/toxicity ratio of cell-cycle phase-specific drugs would be maximized at an integer or fractional multiple of the mean cycle time of the host target populations (this being denoted the "Z-method"). This applies either when mean cancer cell-cycle parameters differ from those of the target host cell population, or when those are similar but the variation in the distribution of their cell-cycle is larger [3,9,10].

It seemed mandatory, already at this level of qualitative understanding of the system, to carefully examine the plausibility of applying the Z-method to cancer and host cells. To this end, a series of laboratory experiments was launched, first examining the effect of drug-pulsing rhythm on cell proliferation, in vitro, and then checking how varying the pulsing rhythm of different drugs will affect disease progression on the level of the whole organism.

Applying an antimetabolite chemotherapeutic drug, Cytarabine (ara-C), to lymphoma cells in vitro, it was experimentally shown that when total drug dose and total treatment duration were kept constant, drug schedules exerting significantly higher cell growth were those possessing periodicity that was an integer multiple of the average population cell-cycle time, as evaluated by rates of DNA synthesis. In equivalent in vivo experiments, mice were treated by short ara-C pulses, having different distributions of the inter-dosing intervals, including stochastically determined periodicity. Toxicity was evaluated by spleen weight, differential peripheral blood measurements, kinetic measurements of bone marrow cell proliferation (with bromodeoxiuridine labeling and flow cytometry analysis) and by overall animal survival. Results of these trials proved the superiority of the Z-method controlling cell proliferation. In particular, it was shown that when the inter-dosing interval is an exact multiple of the inter-mitotic time of bone marrow stem and progenitor cells, cell-cycle kinetics are less affected, myelotoxicity is minimal and survival time of tumor bearing mice is maximal [3-5,11].

The above experiments demonstrate that regimens employing a drug period, which coincides with the inherent periodicity of bone-marrow cells, protect the bone-marrow rather well, leading to increased life-expectancy of cancer-bearing mice. In contrast, other regimens, notably those employing intervals that are randomly distributed around the same mean periodicity, are extremely toxic. In general, this work is a proof of the concept that by using a rational drug scheduling, based on the Z-method, it is feasible to control drug toxicity exerted onto the bone-marrow of cancer-bearing mice, while at the same time delaying their tumor progression. This conclusion has been further supported under more realistic and complex tumor growth models (e.g., [12,13]) and under physiologically-based mathematical models of human hematopoiesis (e.g., [14]).

The above described mathematical models added important new insights on drug treatment strategies, by considering fundamental effects on cellular dynamics. Yet, to enable mathematical tractability, drug-related characteristics were treated very simplistically. For this reason, only qualitative conclusions can be drawn from these model analyses. Now that the proof of concept has been provided, the models are becoming increasingly instrumental in planning concrete treatment strategies. To this end, modeling of the underlying pathological and physiological processes in a patient is wedded with the detailed relevant pharmacokinetics (PKs) and pharmacodynamics (PDs) (e.g., [15,65]). By uniting in one framework the pharmacological properties of the drug with the dynamic properties of the cells in the target tissues, one obtains an improved understanding of how the timing of drug administration, the inter-dosing interval, drug fractionation, and other aspects of

treatment scheduling, may affect the patient. Biomathematics has the power of integrating the vast biomedical and pharmaceutical knowledge into a concise formal language, which enables intensive calculations of the outcomes of complex processes. These calculations, being by far more comprehensive and accurate than any human intuition can be, justify their use for rational treatment design at any stage of the critical path, especially when partial preclinical results collected in several species are to be used for predicting the human response.

36.1.2 Aims of this chapter

In this chapter, we will discuss the application of mathematical modeling tools to elucidate the hematological disorder, thrombocytopenia, in different animal species, and to accurately describe the efficacy and safety of the thrombocytopenia alleviating drugs, thrombopoietin and interleukin-11. Model validation in mice, monkeys and humans, by the use of diverse experimental information, will be discussed, as well and the use of the animal models for predicting human safety and for improving patient treatment.

36.2 Thrombopoiesis

Any mathematical model describing a biological process is based on a verbal model of the process, that is, on an algorithm concisely describing its essential physiological “flow”. We devote this section to a brief presentation of the verbal model of thrombopoiesis, and to the subsequent description of a mathematical model, constituting the essence of platelet development.

36.2.1 Biology

Platelets are components of the hematopoietic system, being the nucleus-lacking derivatives of megakaryocytes (MKs). Platelets function primarily in processes of thrombus formation and vascular repair, but also have roles in natural immunity and metastatic tumor biology. Platelet counts in healthy humans average at 150-400 billion cells per one liter of blood, a homeostasis which is crucial to maintain. Low counts may lead to severe hemorrhage, renal failure, and other disorders, while high counts indicate poor prognosis with respect to cardiovascular diseases and malignancies. Thrombopoiesis, the formation of blood platelets, has been studied for the last century, though critical advances in our understanding of the unique processes that accompany it are only of the last decade. We refer the reader to figure 36.1 for an illustration of the process and to literature for a more elaborate description [16-19].

Normal platelet formation begins with bone marrow progenitors of the lineage, which descend from hematopoietic stem cells and proliferate in response to certain growth factors. The next stages in the sequence involve the immature forms of MKs (promegakaryoblasts and megakaryoblasts), which then develop into larger, mature MKs. As the cells mature into MKs, they gradually lose their ability to divide, but

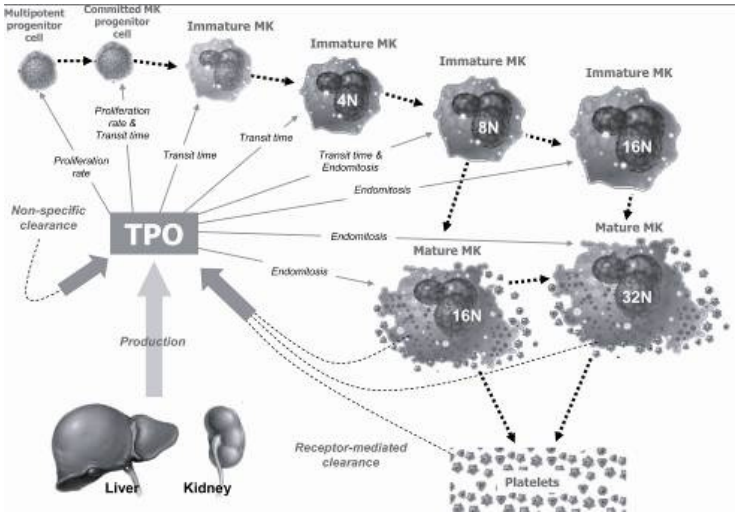

FIGURE 36.1: The process of thrombopoiesis. Uncommited progenitors in the bone marrow (hematopoietic stem cells) proliferate and develop into commited progenitors of the megakaryocyte (MK) lineage, which further develop into immature forms of MKs (promegakaryoblasts and megakaryoblasts). These then develop into larger, mature MKs. Maturation of cells is coupled with loss of the mitotic ability, but endomitosis and polyploidity is maintained until the early stages of MK fragmentation and systemic distribution of platelets. TPO, derived from the liver and kidney constitutively, is a primary mediator of the platelet formation process, and is sequestered by platelets and MKs, as well as non-specifically.

maintain the function of DNA synthesis, thereby undergoing endomitosis and attaining a polyploid state. Finally MK fragmentation occurs, resulting in release of platelets, first to bone-marrow sinusoids and then to the systemic circulation. Radiolabeling studies indicate that the amount of platelets normally consumed by hemostasis is very small and constant. The highly regulated process of platelet consumption is induced by their adhesion to von Willibrand factor (vWF) and extracellular matrix components of damaged blood vessel wall underlying the endothelium. Following platelet adhesion, a clot is formed and the vessel wall is recovered. With a life span of approximately ten days, unconsumed platelets that senesce are removed by macrophages of the reticuloendothelial system, mostly in the spleen.

Thrombopoietin (TPO), a glycoprotein produced by the liver and kidney constitutively and by the bone-marrow upon demand, is characterized as the primary regulator of platelet formation. Though the focus was set on TPO already in the late 60's, it was successfully cloned only in 1992. TPO acts in all stages of thrombopoiesis, its receptors being expressed on each cell type in the lineage. Interestingly, systemic and bone-marrow levels of TPO are inversely correlated to platelet numbers: due to high affinity platelet-bearing TPO receptors, increased

amounts of platelets result in high internalization of TPO, forming successful autoregulation of the thrombopoiesis. It is noted that slightly less significant cytokines, namely the interleukins 3, 6, 11, and stem cell factor (SCF), stromal cell-derived factor 1 (SDF-1) and granulocyte macrophage colony-stimulating factor (GM-CSF), were also identified as modulators in normal platelet formation, each acting in different developmental phases, and some acting in synergy with others. Studies indicate that effects of the surrounding tissue, comprised of fibroblasts, endothelial cells, and macrophages, are also of capability of augmenting thrombopoiesis, though these environmental factors are not thought to be critical since platelets are easily produced also in vitro.

The manipulation of molecular and genetic techniques in the last two decades has greatly boosted the understanding of biological pathways and mechanisms involved in platelet formation. Nonetheless, at the current stage, the regulation of thrombopoiesis, the central molecular components taking part in it, and their significance for therapeutic intervention in platelet-associated illnesses, are yet to be clarified.

36.2.2 Mathematical modeling

Although the intricacies of thrombopoiesis are far from being fully elucidated, current knowledge enabled the verbalization, and subsequently the mathematical formalization of a basic thrombopoiesis-describing model. Schematized in figure 2.2, and elaborated elsewhere, the model divides the entire thrombopoietic lineage into seventeen compartments. Every compartment, except for the first, is represented by time-dependent age distribution, where the number of cells is given as a function of discrete age (time spent in the compartment) and time. The number of cells in the first compartment is a function of time only. There are six groups of compartments in the model, in accordance with the above-mentioned structure of the thrombopoietic lineage. The subdivision of the six groups is as follows: (a) one compartment of lineage-uncommitted progenitors (UCP), (b) one compartment of lineage-committed progenitors (CP), (c) six compartments of endomitotic progenitors (EP), (d) four compartments of developing progenitors (DP), (e) four compartments of MKs, and (f) one compartment of blood-circulating platelets.
The first compartment, UCP, refers to all bone marrow hematopoietic progenitor cells that can differentiate into more than one line (e.g., pluripotent stem cells, CFU-GEMM, etc). We assume one homogeneous UCP population, as its division into various sub-populations is not feasible, since kinetic data regarding the various sub-populations of the UCP compartment (i.e. rates of proliferation, maturation and self-renewal) is rather scarce. In our model, cells of this compartment proliferate at a certain rate (αUCP) and differentiate into MKs or other precursors. Based on previous studies showing that the probabilities of stem cell differentiation into any given hematopoietic lineage are constant, it was assumed that a fixed proportion of mature uncommitted progenitor cells flows into the thrombopoietic lineage (φUCP). Apoptotic cell death may have a significant effect on cell numbers in the proliferating compartments. Thus, we included its effect together with the effect of cell proliferation into the total amplification of cell number in a specific compartment. As currently no information is available concerning apoptosis in the non-proliferating MK compartments, this issue was disregarded in these compartments.

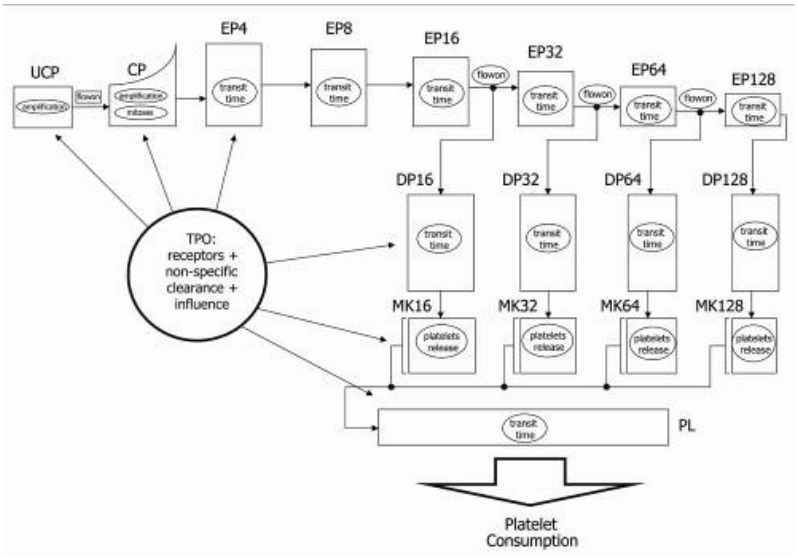

FIGURE 36.2: A scheme of the thrombopoiesis mathematical model. The model consists of seventeen compartments which can be clustered in the following six groups: (a) one compartment of lineage-uncommitted stem cell progenitors (UCP), (b) one compartment of lineage-committed progenitors (CP), (c) six compartments of endomitotic progenitors (EP) of ploidies 4N, 8N, 16N, 32N, 64N 128N, (d) four compartments of developing progenitors (DP) of ploidies 16N, 32N, 64N 128N, (e) four compartments of megakaryocytes (MKs) of ploidies 16N, 32N, 64N 128N, and (f) one compartment of individual, blood-circulating platelets. Relevant key parameters included in the kinetic calculations of the different compartments: amplification rate; flow-on fraction (flowon); transit time; and rate of platelet release. The arrows indicate the direction of inter-compartmental cell flow.

The CP compartment stands for an age distribution of progenitor cells already committed to the thrombopoietic lineage, but still capable of proliferation. The compartment is characterized by a transit time (τCP) and a number of mitoses (Nm). The latter represents the average number of possible cell divisions at that stage. This number may be non-integer, considering that certain cells can be quiescent and undergo fewer mitoses than others. Cells leaving CP enter the first of the six EP compartments, which comprises cells that have lost proliferation ability and yet are not sufficiently mature to release platelets. Thus, this subgroup of compartments, namely EP4, EP8, EP16, EP32, EP64 and EP128, are formed according to the biologically-known sequence of cells of the MK lineage bearing ploidy of 4N, 8N, 16N, 32N, 64N and 128N, respectively. These endomitotic precursors cannot divide, but continue endomitosis. The cells that enter the EP4 compartment are of ploidy 2N, at the exit they have ploidy 4N, and so on for subsequent EP compartments. It is assumed that MKs can release platelets only after reaching the 16N-ploidy phase. Hence to arrive at platelet production in our model, the EP16 compartment must be entered. After cells spend their designated transit time (τEP) in an EP compartment, they can move to the next EP compartment. Fractions of cells that continue endomitosis after moving through EP16, EP32 or EP64 are designated φEP16, φEP32 and φEP64, respectively, where in normal conditions φEP64 = 0.

Alternatively, cells at the EP16, EP32 or EP64 stage may stop the endomitotic process by entering the relevant DP compartment, which is represented by four subgroups of cells. DP cells of 16N, 32N, 64N and 128N ploidy increase their cytoplasmic contents prior to platelet production. Cells that have stopped endomitosis after exiting EP16 compartment enter into DP16; cells that have stopped endomitosis after exiting EP32 compartment enter into DP32, and so forth. After spending a certain amount of time (τDP) in the DP compartment, cells pass to the corresponding MK compartment. The four sub-compartments of this stage signify cells capable of releasing platelets. MK16 compartment receives cells exiting from DP16, MK32 receives cell exiting from DP32, and so on. As in previous compartments, here too the cells are distributed over age (time spent in the compartment), yet there is no predefined transit time. Instead, the new cells entering MK are assumed to have some initial releasing capacity, indicating the number of potential platelets, or total platelets volume, to be released until the cell is exhausted. This capacity is assumed to be larger for cells of larger ploidy. Cells release platelets continuously, and their releasing capacity is consumed until it drops to zero, there upon disappearing from the compartment.

The last compartment, PL, represents platelet counts distributed by age (time spent in blood after the release). Distribution of mean platelet volume (MPV) is also computed in order to allow calculations of platelets degradation. The platelets are readily consumed by the body in an age-independent manner, and in terms of volume (platelets number multiplied by MPV). There is also a maximal life span for old platelets, so that all non-consumed platelets disappear upon reaching a maximal age (denoted by τPL). New platelets appear at every time step, as released by MK cells. This release is also described in terms of volume, and at every time step the amount and MPV are evaluated for the new platelets, taking into account the relative contributions of MK cells of different ploidies.

The formal description of the cellular compartments is supplemented by the model for the endogenous TPO, which regulates the dynamics of the process. A one-compartment PK model for TPO, with a constant production and a linear non-specific clearance, is applied. In addition, there is an alternative, specific clearance of TPO, achieved through the consumption by the cells (receptor binding and internalization). To include this in the model, distributions of receptors per cell in all the line-committed compartments (CP and the groups that follow) are incorporated. Formulae are constructed for receptor numbers distributed over cell age. Receptors, constantly produced by the cells, excluding platelets that have no nucleus, bind free TPO and are internalized. To reflect the non-specific clearance of TPO, Michaelis-Menten behavior is assumed for TPO-receptor kinetics.

The major stabilizing feedback in the model is exerted via the effects of TPO on the cells throughout the lineage. Kinetic parameters of the model's compartments are functions of TPO concentrations; In the UCP compartment, the amplification rate is an increasing function of the TPO concentration. Similarly, the number of mitoses in the CP compartment is an increasing function of TPO. In contrast, the transit times in CP, EP, and DP, and the EP flow-on (fraction of cells that continue endomitosis) are decreasing functions of the TPO concentration. Finally, the MPV of released platelets (and consequentially, the loss of cell volume) is an increasing function of the TPO concentration in the MK compartments. For all the dependencies listed above, sigmoid functions with saturation for large values of TPO concentration are used. In addition to this feedback, a TPO-independent feedback on cell proliferation in the model, or a "crowding effect", is included as well. The amplification rate in UCP and number of mitoses in CP are decreasing functions of cell numbers in these compartments, respectively. This represents

internal regulation of cell proliferation in these stages. Such functions are also assumed to have a sigmoid form.

The model is mathematically formalized according to the above description, using discrete difference equations. The variables of the model (e.g. cell numbers) are represented as functions of discrete time-points, with a certain step Δt. The set of the model equations describes the recursive calculation of the system state for the current time point, using the state of the system at previous time points. For the specific clearance model, steady-state approximations are used, as these processes are on a much faster time-scale than all the rest of the model. The model is simulated using a C++ code, and its parameters are estimated either directly from experimental measurements, or by fitting the model to the published experimental data. The validation of the model is further described in section 5.

36.3 Thrombocytopenia

Setting the essential rules for depicting thrombopoiesis, as explained in section 36.2, it is possible to evaluate not only the homeostatic behavior of the system, but also its irregularities. Diversion from normal steady state thrombopoiesis can arise from various reasons, and can have several physiological consequences. In this section, we will discuss some of the main mechanisms leading to low platelet count, termed thrombocytopenia (TP). Both current and future therapeutic avenues will be illustrated.

36.3.1 Pathophysiology

The concise summary of TP pathophysiology, presented in this section, is based on extensive reviews of this pathology in the current hematology literature, notably [16,20,21]. The clinical significance of TP, characterized by a blood platelet count of less than 150,000 cells per microliter, stems from the major role of platelets in the process of normal hemostasis. Low platelet counts lead to diminished ability of hemostasis, and onsequently, increased bleeding propensity. Yet there are important exceptions to this rule. Firstly, clinically significant bleeding occurs regularly only when the amount of platelets decreases beyond 10-20,000/μL. Secondly, exact clinical manifestation of this disorder depends on the underlying pathophysiological mechanisms: While TP induced by low platelet production leads to increased risk of bleeding, TP caused by excessive platelet consumption may result in an elevated risk of thromboembolism.

TP can be caused by one, or more, of the following mechanisms (elaborated in the following section): (a) decreased platelet production, (b) increased sequestration of platelets, or (c) their accelerated destruction. TP induced by the first mechanism, impaired production of platelets, accompanies a variety of bone marrow pathologies. Congenital hereditary decreased production-TP, one of these cases, is very rare. It can be caused by malfunctioning TPO receptor signaling (e.g., amegakaryocytic TP) or by impaired MK fragmentation into mature platelets. The more common syndrome is acquired decreased production TP. This form of TP can be a result of pathological bone marrow infiltration in hematopoietic malignancies (leukemias and lymphomas) or in massive metastases of extramedullary solid tumors. Alternatively, this could occur in myelodysplastic syndromes and vitamin B12 deficiency, when intrinsic maturation defects arise in the early hematopoietic progenitors, with involvement of 1-3 hematopoietic lines. Extrinsic inhibitors of hematopoietic progenitor proliferation, such as (a) cytotoxic drugs (anticancer chemotherapy), (b) circulating auto-antibodies to MKs (immune thrombocytopenic

purpura, systemic lupus erythematosus, etc.), (c) proinflammatory cytokines (sepsis), or (d) various viral infections (EBV, CMV, HIV, etc.), can induce this TP form as wells.

Increased sequestration-TP, the second mechanism, is a common finding in splenomegaly of any cause. A frequent consequence of splenic enlargement is increased pressure in the portal vein, which causes draining of blood from the spleen into the liver. This syndrome, referred to as portal hypertension, is present in a variety of chronic liver diseases and in cases of portal vein thrombosis due to hypercoagulation states. In portal hypertension, increased sequestration is often the only cause of TP. Other diseases with splenomegaly generally produce TP of a combined etiology. For example, splenomegaly is associated with conditions of leukemia and lymphoma, in which bone marrow infiltration results in decreased platelet production. Similar combinations of TP mechanisms appear in several infectious disorders (e.g. brucellosis and visceral leishmaniasis) and inflammatory diseases (e.g. Felty's syndrome and systemic juvenile rheumatoid arthritis).

Pathologically accelerated platelet destruction (the third mechanism of TP) can be induced by either increased consumption, or by physical factors. Physical platelet destruction occurs upon increased blood shear stress near valvular and intravascular prosthetic devices. There are varying disorders of increased platelet consumption by pathological uncontrolled coagulation. Thrombotic thrombocytopenic purpura (TTP) and hemolytic uremic syndrome (HUS) are associated with thrombosis, rather than bleeding, despite low platelet count. Recent progress in TTP research reveals that the underlying pathology involves decreased or absent function of a protease known as a disintegrin and metalloproteinase with a thrombospondin type 1 motif, member 13 (ADAMTS13), responsible for specific cleavage of vWF. As a consequence, large multimers of vWF are formed, and they initiate bouts of platelet adhesion and activation. Conversely, pathogenesis of HUS is incompletely understood. Since this disorder appears typically after certain bacterial infection, it is assumed that cross-reactive antibodies are responsible for platelet activation in this syndrome. Disseminated intravascular coagulation (DIC), distinct from the latter two disorders by its simultaneous induction of both thrombosis and bleeding, is a common feature of several severe illnesses including overwhelming sepsis, poisoning due to snake bites, amniotic fluid embolism and fat embolism. The pathogenesis of DIC includes uncontrolled activation of intravascular coagulation pathways, leading to increased platelet consumption.

Accelerated destruction-TP can also be attributed to immunological disorders. The most recognized disorder of this type is immune (idiopathic) thrombocytopenic purpura (ITP). The underlying pathology consists of formation of auto-antibodies against specific platelet surface antigens. Platelets covered with autoantibodies are effectively and prematurely destroyed by the phagocytes of the reticuloendothelial system. In the minority of cases, presence of auto-antibodies to MKs is also suspected, which results in TP of mixed etiology – both decreased production and accelerated destruction. Other diseases with autoimmune platelet destruction include systemic lupus erythematosus and antiphospholipid antibody syndrome. Drug-induced immune TP was observed upon the use of many exogenous factors, including heparin, gold, antibiotics and anti-inflammatory drugs. In these cases, antibodies are formed against the complex of a drug with platelet surface antigens. In heparin-induced TP, thrombotic complications are common (similar to those in TTP), since antibodies lead to excessive platelet activation in addition to increased clearance.

To examine the risk of TP in new drugs, or in yet to be tried drug regimens, the PK and PD of the drug should be simulated superimposed on a mathematical model of

the underlying TP mechanism. However, how to determine the specific TP mechanism in each particular case is a very challenging task. While certain clues can be received from patient's medical history, physical examination and peripheral blood smear, bone marrow biopsy is frequently required in order to evaluate number of MKs. Low numbers are indicative of decreased production, while increased numbers are associated with accelerated destruction. Some cases remain undefined, even after thorough laboratory investigation and manipulation of extensive tools. The type of TP guides both further clinical work-up for specific underlying pathology, as well as possible treatment options.

36.3.2 Current therapy

In light of the different mechanisms for TP, treatment is diverse and highly dependent on the underlying cause. Generally, we can divide current therapy into treatments directed against pathophysiological mechanisms, and symptomatic treatment of TP-induced bleeding/thrombosis. In the majority of the cases, platelet counts do not drop below 10-20,000 per microliter of blood, so that serious bleeding complications do not develop. Treatment of the underlying causes includes withdrawal of the offending stimulus, e.g. discontinuation of an immunogenic drug, removal of vWF complexes by plasma exchange in TTP, replacement of mechanical prosthesis by a biological one, and also includes specific treatment of malignancies and infections.

It is imperative to identify accelerated platelet destruction by the reticuloendothelial system, for which splenectomy and/or administration of intravenous immunoglobulins (IVIG) is indicated in refractory cases. Splenectomies lead to decreased auto-antibody production, and remove a large fraction of phagocytes responsible for platelet destruction. IVIG, on the other hand, saturates antibody-binding receptors on the phagocytes and suppresses their interaction with antibody-covered platelets and MKs. Therefore, theoretically IVIG should be more effective in cases of MK-specific antibodies. This hypothesis, however, has not been examined clinically, due to technical difficulties in identifying antibody specificity in particular patients. Importantly, neither a splenectomy, nor IVIG therapy, are effective in cases of direct complement-mediated antibody toxicity to platelets and MKs.

Symptomatic treatment of TP-associated bleeding disorders consists mainly of transfusion of donor platelets. Platelet transfusions are commonly used, with approximately 9 million units yearly applied in the US alone. Though repeated platelet transfusions may aid in preventing bleeding, they can transmit both viral and bacterial infections, and cause alloimmunization which requires HLA-matched donors. Health care costs and inconvenience to patients also pose a concern. Furthermore, this treatment must be repeated on a regular and frequent basis, due to the short half-life of donor platelets (3-4 days), and since the underlying causes of TP are left untreated. Platelet transfusions are of especially low efficacy in immunologically-mediated TP that involve an even shorter platelet half-life.

36.3.3 Novel cytokine therapy

Over the past 15 years, attempts to find new therapies to replace platelet transfusions in the treatment of thrombocytopenic disorders have naturally been focused on the growth factors involved in normal thrombopoiesis (see section 36.2). Interleukin (IL)-11, discovered in 1990 to be a thrombopoietic growth factor secreted from bone-marrow stromal cells, was the first candidate for this purpose. The genetically-engineered form of this protein, recombinant human IL-11 (rhIL-11) was evaluated for treatment in patients with non-myeloid malignancies that suffered from chemotherapy-induced thrombocytopenia, and did, in fact, produce a dose-dependent increase in platelets. RhIL-11, approved in 1997 for prevention of severe drug-induced thrombocytopenia, is currently the only cytokine licensed in the US for this purpose. However, with its only modest thrombopoietic activity and its use often associated with intolerable side effects, IL-11 has not satisfied the demands for an efficacious thrombopoietic agent to be applied in the clinical setting [22-24].

In light of the central role of TPO in the proliferation and survival of MKs and increased platelet production, its potential to replace standard platelet transfusion therapy and improve platelet harvesting efficacy in donors seems even greater than that of IL-11 [22,25]. Recombinant human TPO (rhTPO) has been examined for exogenous application in patients with initial thrombocytopenic disorders, as well as for treatment of chemotherapeutically-induced myelosuppression in cancer patients. However, phase 1 studies with rhTPO in healthy individuals remain disappointing: In a trial that was aimed at improving platelet yields in donors, some of them developed immune-mediated TP due to appearance of auto-antibodies to native TPO. Evaluation of rhTPO therapy has also encountered difficulties due to delayed peak platelet response and neutralizing antibodies formed against the pegylated molecule. It is believed that most complications are caused by significant antigenic differences between the native and recombinant TPO proteins. As a result, this molecule currently remains in its developmental stage, and is not yet approved. Small TPO analogs and synthetic TPO-derived agents are currently being developed to bypass immunogenicity-related problems [26-34].

Mathematical modeling of thrombopoiesis (as described in section 36.2) and drug-induced TP (as will be shown in section 36.6) can aid in disentangling disease dynamics and in deciphering pathophysiological mechanisms underlying the disease. In particular, mathematical models of TPO-affected thrombopoiesis and of IL-11-induced side-effects, enable to propose improved treatment schedules for both drugs, obtaining maximum efficacy and substantially improved safety (see section 36.4 and 36.5). In turn, preclinical validation of these improved regimens can give new hope for clinical application of these cytokines in their multiple arenas.

36.4 Modeling drug effects on thrombopoiesis

Innovative cytokine-based therapeutics of IL-11 and TPO (see section 36.3) developed for application in thrombopoiesis-related syndromes and for efficiently harvesting donor platelets have been extensively studied in the last decade or so. Yet, even today, toxicity-related limitations of each of these molecules prevent their clinical applicability. The following section will be dedicated to mathematical models focusing on both beneficial and detrimental consequences of these therapeutic avenues, and on the manner by which such models may be used to suggest improved treatment strategies.

36.4.1 Toxicity modeling: Interleukin (IL)-11:

Though IL-11 treatment has been approved for treating drug-induced TP for almost a decade, its induction of intolerably toxic effects has proved to crucially impede its therapeutic use. The cytokine has been shown to elicit a wide range of side-effects, mainly associated with blood volume expansion (BVE). These include complications of various grades of edema, anemia, pleural effusion, cardiac arrhythmia, etc [23].

An initial and generalized perspective on this issue required a mathematical model of IL-11-induced BVE. However, the definitive mechanism underlying IL-11-mediated water accumulation is yet to be discovered, and the incomplete data [23, 35], restrict the possibility to produce a concrete and reliable model for this problem. Instead, a novel biomathematical approach was developed so that not one, but several mathematical models, each representing an alternative mechanism for BVE following IL-11 therapy, were devised and evaluated [36]. The underlying assumption here was that by concurrently simulating multiple models, which formally describe alternative mechanisms, but all producing the same fluid-retentive behavior, it is possible to faithfully depict this effect despite the obscurity of the actual mechanism and related data. Accordingly, convergence of all models to yield unified BVE dynamics was the characteristic by which their success and predictive ability was measured. Furthermore, since the range of different models that capture the behavior of stable biological systems, e.g., body water homeostasis, is assumed to be relatively narrow, the chances of arriving at a reliable model was considered even greater in the drug-afflicted BVE setting [36].

Three closely-related biologically-based models were constructed using ordinary differential equations (ODEs) and standard Michaelis-Menten kinetics. The models incorporated basic water regulation properties (blood volume, pressure and vascular compartments) and endocrinal feedback effects (compartments for BVE-upregulating and downregulating hormones), together with the IL-11-induced perturbation of the system. Notably, a short-term neuronal influence or long-term permanent structural changes were not considered, restricting the modeling to the therapeutic time scale. The variation between the different models was expressed in (a) the component directly affected by IL-11, being either blood volume or blood vessels, and (b) the components affected by the endocrinal hormones, being both vessels and volume (full effect) or only volume (partial effect). Thus, model 1 assumes IL-11-induced vessel enlargement and full endocrinal feedback; model 2 assumes IL-11-induced volume expansion and full endocrinal function; model 3 assumes IL-11-induced volume expansion and partial endocrinal function. The models were identical in all other assumptions.

Dynamics of subcutaneously-administered IL-11 were represented by a one-compartment PK model, with first order absorption from the external tissue. IL-11 concentrations in the tissue (I_T) and plasma (I_P) are given by

$$\dot{I}_T = -c_1 I_T \quad (36.1)$$

and

$$\dot{I}_P = fc_1 I_T - c_2 I_P \quad (36.2),$$

where $I_T(t=0)$ is the administered IL-11 concentration, and $I_P(t=0)=0$. The coefficient c_1 denotes the rate of drug transport from the primary tissue to the plasma, c_2 is the drug clearance rate, and the fraction of transferred drug, an indicator of bioavailability, is f.

Blood pressure was described by considering its classical correlation to heart rate, stroke volume and systemic vascular resistance. As heart rate variability was disregarded in experiments, and an inverse relationship between vascular resistance and vascular capacity was assumed, blood pressure was described to be a function of blood volume and the vascular capacity (expressed in terms of vessel surface):

$$P(t) = \left(\frac{V(t)}{S(t)^{3/2}} \right)^{n_0} \quad (36.3)$$

The function P(t) is blood pressure at time t, S(t) denotes overall vessel surface at time t, V(t) is blood volume at time t, and n_0 is a parameter. Steady state values of pressure, overall vessels surface and volume were given by P_{st}, S_{st}, and V_{st}, respectively.

Dynamics of the BVE-upregulating hormones (H_U), and the BVE-downregulating hormones (H_D) were subjected to blood pressure variations, and were therefore given by

$$\dot{H}_U = \alpha_1 g\left(P_{st} - P(t)\right) - d_1 H_U(t) \quad (36.4)$$

and

$$\dot{H}_D = \alpha_2 g\left(P(t) - P_{st}\right) - d_2 H_D(t) \quad (36.5),$$

respectively. The description is general, and does not refer to hormonal concentrations per se, but rather, to effects associated with endocrinal deviations. In equations 36.4 and 36.5, formation rates (α1, α2) and degradation rates (d1, d2) of the endocrinal effects were taken as constants, and blood pressure deviations from steady state allowed formation of each factor using the function

$$g(x) = \begin{cases} x & \text{if } x>0 \\ 0 & \text{if } x\leq 0 \end{cases} \quad (36.6).$$

The vascular structure was described in two-dimensional units, e.g. by relating to the average surface of the inner endothelium layer of blood vessels. IL-11-induced vessel surface enlargement (in model 1) and HU-induced vasoconstriction or HD-induced vasodilation (in models 1 and 2), were described by biologically-compatible non-linear functions. As described earlier, model 3 does not enable

vascular resizing in response to IL-11 or hormones. All three models, however, incorporate simple intrinsic feedback effects to vessel steady-state in blood vessel dynamics. Thus, the equation for models 1, 2 and 3 are given by 36.7, 36.8 and 36.9, respectively.

$$\dot{S} = \frac{\beta_0 (I_P(t))^{r_0}}{k_0 + (I_P(t))^{r_0}} - \frac{\beta_1 (H_U(t))^{r_1}}{k_1 + (H_U(t))^{r_1}} + \frac{\beta_2 (H_D(t))^{r_2}}{k_2 + (H_U(t))^{r_2}} + \beta_3 (S_{st} - S(t)) \quad (36.7),$$

$$\dot{S} = -\frac{\beta_1 (H_U(t))^{r_1}}{k_1 + (H_U(t))^{r_1}} + \frac{\beta_2 (H_D(t))^{r_2}}{k_2 + (H_U(t))^{r_2}} + \beta_3 (S_{st} - S(t)) \quad (36.8),$$

and

$$\dot{S} = \beta_3 (S_{st} - S(t)) \quad (36.9).$$

Vascular modification rates in response to IL-11, HU, and HD are denoted as b_0, b_1 and b_2, respectively, and b_3 is the coefficient of direct vessel surface regulation. Parameters k_0,k_1,k_2 and r_0,r_1,r_2 are positive.

Volume dynamics were initially characterized by water absorption-excretion differences. Absorption rates were assumed not to deviate from steady state values, whereas excretion rates were taken as susceptible to (a) systemic blood pressure deviations, known to specifically act on renal water excretion, and to (b) the IL-11-induced effects. The function of blood volume was therefore described by the difference between absorption rates, which were constant (Ast), and excretion rates, which were set as the pressure-related difference between normal steady-state excretion (Est) and the excretion in the IL-11 scenario (Edrug):

$$\dot{V} = A_{st} - \left(\frac{P(t)}{P_{st}}\right)^{n_1} (E_{st} - E_{drug}(t)) \quad (36.10)$$

The power coefficient n_1 sets the strength of the dependence of the volume changes on the pressure variation. Assuming equal steady state absorption and excretion rates (A_{st}=E_{st}) under normal conditions, equation 36.10 turns into

$$\dot{V} = E_{st}\left(1 - \left(\frac{P(t)}{P_{st}}\right)^{n_1}\right) + \left(\frac{P(t)}{P_{st}}\right)^{n_1} (E_{drug}(t)) \quad (36.11).$$

Excretion of volume in the therapeutic scenario (i.e. the term Edrug) was assumed to be affected by the hormones in all three models. As described above, in models 2 and 3 it was additionally assumed that the drug directly influences volume excretion. Both of these effects (IL-11 and hormone mediated) were assumed to be non-linear, and introduced into the volume dynamics given in equation 36.11. For model 1, this gave

$$\dot{V} = E_{st}\left(1 - \left(\frac{P(t)}{P_{st}}\right)^{n_1}\right) + \left(\frac{P(t)}{P_{st}}\right)^{n_1} \left(\frac{\gamma_1 (H_U(t))^{q_1}}{m_1 + (H_U(t))^{q_1}} - \frac{\gamma_2 (H_D(t))^{q_2}}{m_2 + (H_D(t))^{q_2}}\right) \quad (36.12),$$

while for models 2 and 3, the equation was

$$\dot{V} = E_{st}\left(1-\left(\frac{P(t)}{P_{st}}\right)^{n_1}\right)+\left(\frac{P(t)}{P_{st}}\right)^{n_1}\left(\frac{\gamma_0\left(I_P(t)\right)^{q_0}}{m_0+\left(I_P(t)\right)^{q_0}}+\frac{\gamma_1\left(H_U(t)\right)^{q_1}}{m_1+\left(H_U(t)\right)^{q_1}}-\frac{\gamma_2\left(H_D(t)\right)^{q_2}}{m_2+\left(H_D(t)\right)^{q_2}}\right)$$

(36.13).

The IL-11, HU and HD -afflicted rates of water excretion are denoted g_0, g_1 and g_2, respectively. Parameters m_0,m_1,m_2 and q_0,q_1,q_2 are positive constants.

Subsequent calibration of the models was accomplished by obtaining and utilizing data from a human study of IL-11 safety, and their predictive ability was evaluated under different regimens of IL-11 therapy. These stages of the work are further described in section 36.5.

36.4.2 Efficacy modeling: Thrombopoietin (TPO)

As we have illustrated in section 36.3, platelet deficiencies hamper the development of improved therapeutic regimens for hematology and oncology patients, as well as in their clinical management [22,27]. The possible use of TPO to abrogate these disorders has also been debated (section 36.3). The PK of rhTPO therapy was mathematically modeled in terms of ODEs, and solved numerically using the Euler method. This extension was simulated in conjunction with the thrombopoiesis model described in section 36.2 (see also [37,38]). The independent PK model for rhTPO was similar in its structure to that of endogenous TPO, though the kinetic parameters were assumed to be different. The reason for this lies in the fact that exogenously-administered synthetic molecules have been shown to differ from the endogenous analogs in a number of characteristics [32]. The model extension also assumes competitive binding of TPO and rhTPO to cell receptors. When describing the PD of the drug, its effects were considered similar to those of the endogenous protein, the latter already existing in the model. Parameter calibration of the model, as well as its retrospective and prospective validation in different species, is detailed in section 36.5.

36.4.3 Modeling combination therapy: chemotherapy and TPO support

The consideration of TPO as a potential candidate for alleviating chemotherapy-induced TP in patients with malignant disorders (see section 36.3) introduces the issue of combination therapy. The addition of TPO to a cytotoxic-drug affected scenario, allowing restoration of the damaged thrombopoietic system, can be described via minor manipulation of the basic mathematical model. To do this, one should take into account the effect of chemotherapeutic drugs on the thrombopoietic lineage. Chemotherapy nonspecifically damages all dividing cells, particularly progenitor cells of the thrombopoietic lineage. These targets are represented by the UCP and CP compartments of the TPO model (section 36.2). Accordingly, the model assumes that the cytotoxic drug eliminates dividing cells in a concentration-dependent manner, and, possibly (depending on the drug), in a cell-cycle phase specific manner. The model incorporates the PK of the drug, to obtain the time course of drug concentrations in blood and the bone marrow. Subsequently, a PD model for this drug is applied: the apoptosis probability of a

dividing cell is calculated as a function of its position in the cycle and of the current drug concentration.

After constructing such a model and validating it, drug developers and treating physicians can explore the unlimited space of possible conjugate treatments, in which the side effects of chemotherapy are suppressed by use of exogenous TPO. The model allows examining different treatment regimens, predicting their possible outcomes and selecting the best possible treatment strategies, while avoiding adverse effects, such as those observed in clinical trials of TPO. This identification of improved treatment strategy can be done for the general population, as well as on patient-specific basis, the latter requiring the specific model parameters of the treated patient, which can be evaluated using the individual platelet profiles post drug intervention.

36.5 Using the validated model for predicting improved efficacy/toxicity profile

As explained in section 3, clinical evaluation of IL-11 and TPO was obstructed due to safety problems. It was therefore imperative to investigate the mathematical models of TPO-mediated thrombopoiesis and IL-11-induced fluid retention (sections 36.2, 36.4), in order to suggest how to overcome the limitations involved in the development of these drugs. We will show in this section how species-specific model parameters can be evaluated and the means by which retrospective and prospective validation of the mathematical models is achieved. Thereafter we will discuss model use for predicting improved chemotherapy and supportive administration regimens.

36.5.1 Model validation by retrospective human study results: IL-11 and TPO

Since modeling IL-11-mediated BVE has employed the specially-developed multiple modeling approach (see section 36.4), the above-depicted diverse models are considered validated and of predictive capability only upon their arrival at unified volume dynamics. The study therefore consisted of two essential steps: experimentally-based calibration and parallel assessment of model simulation-derived BVE behavior. These procedures are described hereafter [36].

In the first stage, model parameters were successfully calibrated to retrospectively retrieve clinically-evaluated, blood volume measurements following daily IL-11 administration of 25 μg/kg doses to healthy volunteers for a week [35]. The data that served for approximation were collected during the first week, that is, within the therapeutic time frame. However, subsequent simulations of the models under the same regimen failed to generate unified behavior of BVE dynamics (figure 36.3, upper panel). In contrast, when simulations were preceded by calibration of the models using data from stages both within therapy (the first week), and up to one month following treatment termination, the output dynamics were highly similar between the models (figure 36.3, lower panel). In fact, the observed high correlation between the numbers of experimental points used for model calibration, and models' increased similarity (data not shown), strengthened the possibility that by using more data points, model similarity and thus reliability and clinical predictability, can be improved.

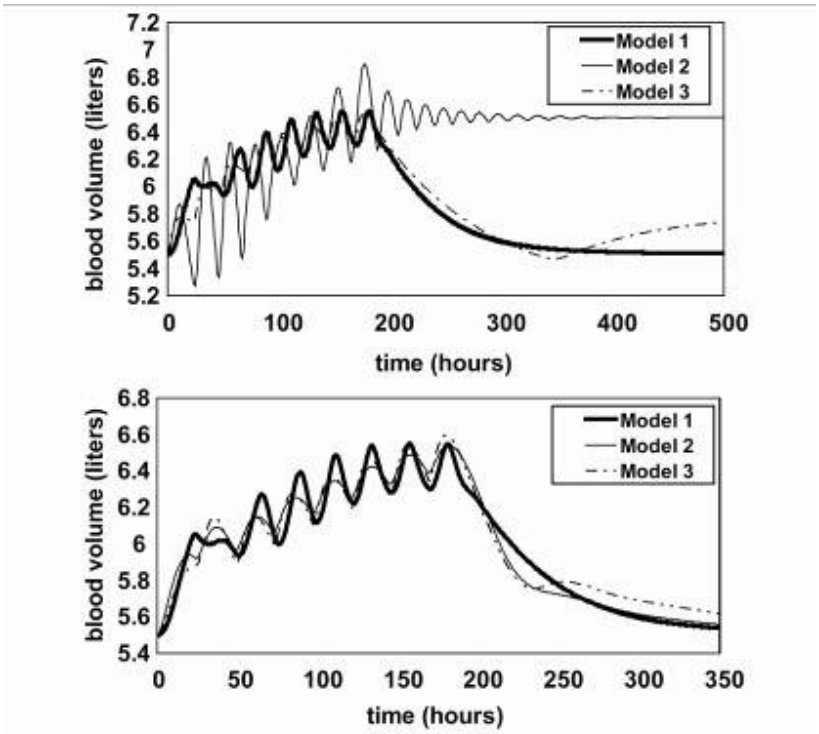

FIGURE 36.3: Comparison of alternative mathematical models for BVE dynamics following calibration by results of a clinical IL-11 study. Blood volume (liters) measured during one week of IL-11 therapy (7 daily doses of 25 μg/kg), was taken from a previous study in healthy humans. Three models, calibrated with data from either the therapeutic days (upper panel), or both the therapeutic and post-therapeutic windows (lower panel) were simulated under the above experimental treatment schedule (data adapted from [36]).

In the second stage of the work, the predictability of the models was evaluated in a wider therapeutic spectrum. The models were simulated under IL-11 treatment strategies of various durations, various inter-dosing intervals and various dose intensities, where model-derived dynamics were again compared to assess the model robustness in portraying BVE dynamics. Highest values of similarity between models, as shown by the difference index, were observed when the average IL-11 dose per day of the tested treatment was close to that of the experimental treatment of daily 25 μg/kg doses (see figure 36.4, as an example). This suggests that in this example of obscure toxicity mechanism, one can trust the model-derived BVE predictions for various IL-11 treatments, provided their average daily dose of IL-11 is in proximity to that used in the original clinical experiment.

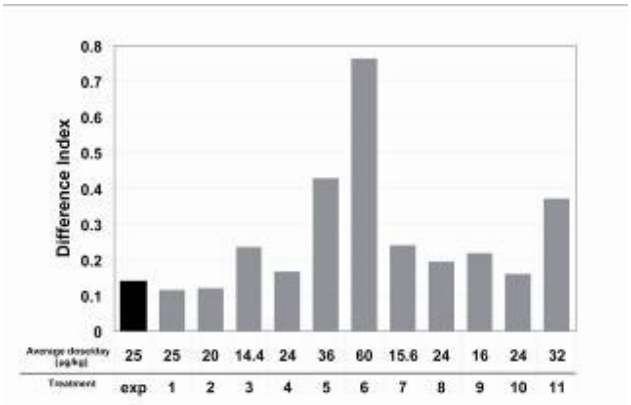

FIGURE 36.4: Model-derived BVE dynamics in therapeutic regimens that are close to experimental schedules in average dose per day values. Model simulations under the experimental schedule (treatment 'exp') and other regimens of various durations, doses, and inter-dosing intervals (treatments 1-11), following calibration with clinical measurements, are compared using the difference index (data adapted from [36]).

The mathematical method applied in the case of IL-11 shows that given preliminary experimental data from various stages of therapy, beginning at phases within the therapeutic window and ending at the recuperated steady-state, the different models reliably predict dynamics of water retention within a certain span of IL-11-administration strategies. Considering the recommended IL-11 levels (10-100 μg/kg/day), and the above model-derived conclusions, clinical studies evaluating BVE within concentrations of 10, 20, 30, etc. μg/kg/day are required to form a complete predictability frame of BVE within all relevant treatment scenarios. This would then allow appraisal of the clinical applicability of each of these IL-11 therapy schedules, as well as others.

As in the above-presented process of IL-11 model evaluation, clinical information was used for the TPO case. A thrombopoiesis computational model was designed on the basis of the mathematical descriptions of TPO-induced thrombopoiesis (elaborated in sections 36.2, 36.4), to enable simulation and evaluation of in vivo platelet formation and to suggest therapeutic TPO regimens of improved efficacy and reduced immunogenicity [38]. The computer model was adjusted and validated for both murine, simian and human, as will be elaborated below.

Currently human validation of the thrombopoiesis computer model is possible only in retrospective, as the drug has not yet undergone the appropriate regulatory procedures enabling human administration. To retrospectively validate the model it was calibrated using a set of biologically realistic parameter values, so that homeostatic behavior, i.e. a normative count of 320,000 platelets/□l blood, was retrieved in untreated conditions. Next, simulation of the computerized model under recombinant human TPO (rhTPO) administration was carried out. Data from a clinical trial [39], which included PK information (i.e. rhTPO concentration in blood) and accurate platelet counts in response to different TPO dosages, served the calibration process: Three patients were assigned to a single IV bolus administration of each of the four dosages 0.3, 0.6, 1.2 or 2.4 □g/kg. The three platelet count curves for each dosage were averaged and a single parameter set, which enabled the model to accurately retrieve platelet dynamics observed under

the various treatment regimens, as shown in figure 5.3, was identified. This parameter set was determined as the representative for the "average patient".

While TPO therapies pose many questions, such as its effects on elevated platelet counts in clonal thrombocytosis, the opposite problem, namely that of reduced platelet counts, introduces equally significant challenges. Since TP is a common dose-limiting side effect of cancer chemotherapeutics, as discussed in sections 36.3 and 36.4, accurate predictions of the chemotherapeutically reduced platelet dynamics are of importance when planning treatments. To allow predicting effect of cytotoxics on thrombopoiesis in individual patients, the average “Virtual Patient” was tested for its ability to retrieve the outcomes of a standard chemotherapeutic treatment by doxorubicin. The model was successfully calibrated in reference to clinical published experimental data [40], as shown by figure 36.3 (lower right panel) and improved TPO regimens were suggested. Prospective validation of the generality and clinical predictability of the model is warranted. A different biomathematical approach, elaborated in section 36.7, uses data from human and animal cell culturing and from preclinical studies that are available in the pharmaceutical industry, in order to develop therapeutic strategies with minimal suppression of thrombopoiesis.

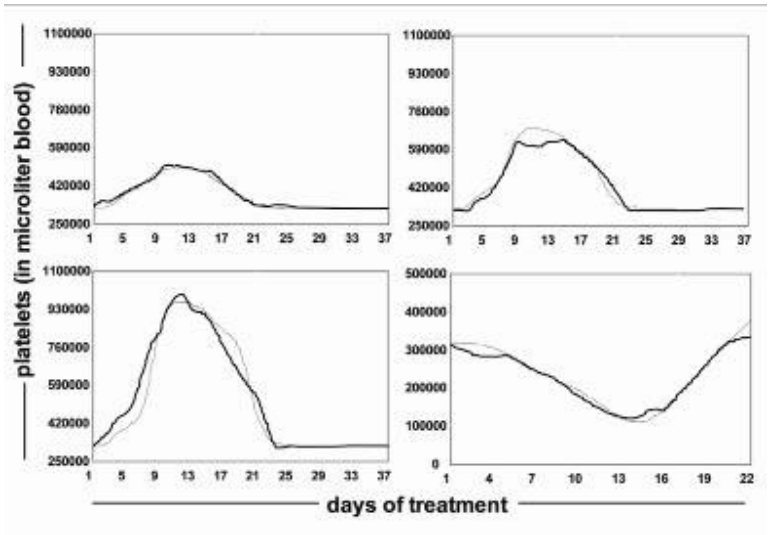

FIGURE 36.5: Model predictions of platelet profiles in patients treated by TPO and chemotherapy compared to clinical results. Average platelet counts in human patients are plotted, following a single IV bolus rhTPO administration of 0.3 □g/kg (upper left panel), 1.2 □g/kg (upper right panel), or 2.4 □g/kg (lower left panel), or an IV infusion of doxorubicin for three days, the total dose being 90 mg/m2 (lower right panel). Simulation-generated curves are shown by thick lines; clinical results are shown by thin lines.

In conclusion, the thrombopoiesis computer model was successfully calibrated to accurately retrieve relevant clinical information reflecting TPO therapy, as well as to chemotherapy, but it is yet to undergo prospective human validation. Importantly, the models described here for different thrombopoietic growth factors are each targeted towards opposing aspects of therapy: while the IL-11 mathematical model attempts to define the toxicity associated with drug-induced alleviation of TP, the computerized-TPO model is aimed at accurately predicting the direct beneficial results of such therapy on platelet restoration.

36.5.2 Model validation in prospective animal trials: TPO applied to the Virtual Mouse and Virtual Monkey

To use the model predictions for clinical decision-making, one must still substantiate the superiority of the model-suggested improved TPO regimens. This task must be carried out in animals first, not only due to safety issues, but also because typically in such cases, the agent in question is not yet approved for the treatment of patients. Once a proof of concept in animals is provided for its power to suggest improved regimens, the model can become instrumental during the clinical phases of drug development, for avoiding excessive and unnecessary toxicity and for reducing the number of patients in Phase I of the clinical development. These steps are expected to pave the road for routine clinical use of the computer-based prediction tool.

The underlying assumption in this work was that improved TPO schedules are those employing the smallest drug doses required to achieve the desired efficacy. This assumption is based on a biomathematical study which examined the effect of dose intensities on drug immunogenicity. Results of this work suggest that for given immuno-reactive system, there exists a critical drug dose for which the relevant immunogenic threshold is expected to be exceeded, thus affecting patient health [15].

To validate the model's predictions in preclinical experiments with BALB/C mice and Rhesus monkeys, the thrombopoiesis model was calibrated to reflect murine or simian thrombopoiesis. This was achieved by using literature-derived data. The species-adapted models, "Virtual Mouse" and "Virtual Monkey", were subsequently used to adjust the improved TPO treatment to the species in question, and test this treatment in animal experiments. This work is described hereafter [41].

Parameter calibration of the thrombopoiesis computer model was performed for fine-tuning the model to accurately describe thrombopoiesis in each species. This work involved definition of a biologically realistic range of values for each parameter in murine thrombopoiesis [28,42-47] and simian thrombopoiesis [22,48-54], which were then entered as the initial parameter values, subsequently to be fine-tuned according to the specific tested population. Ability of the model to retrieve platelet profiles in each animal group was then tested.
Next, the prediction accuracy of the thrombopoiesis computer model was validated in mice. Specifically, simulating the model it was predicted that platelet counts, similar to those achieved with the accepted TPO administration schedule can also be generated under different schedules of appreciably reduced TPO doses (figure 36.6, upper panel). Hence, two different administration regimens were

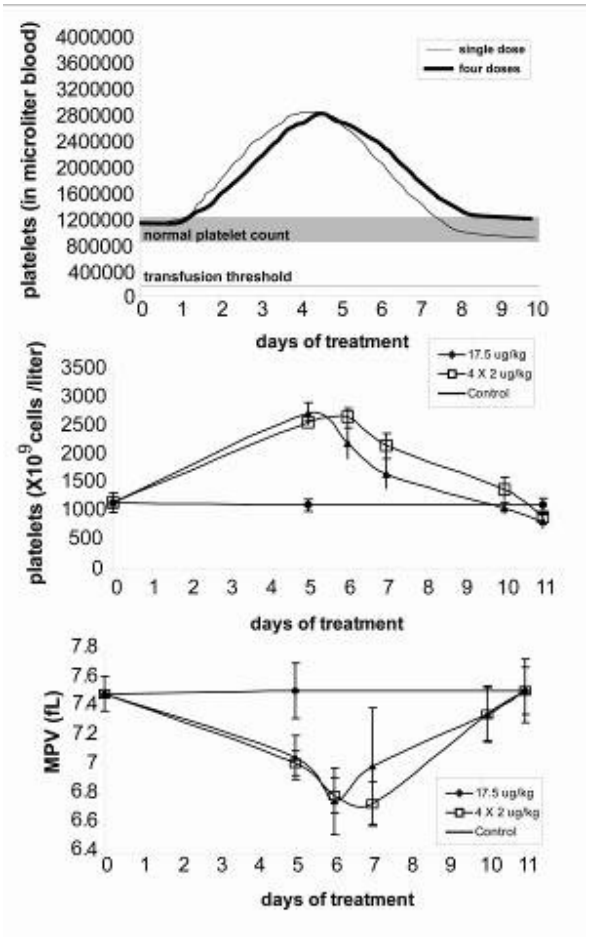

FIGURE 36.6: Model predictions of platelet profiles in mice treated by TPO as compared to experimental results. Upper panel: The thrombopoiesis model-generated predictions indicating similar efficacy in platelet formation between a "conventional" single dose TPO treatment of 17.5 □g/kg, and a model-suggested reduced TPO treatment of four daily doses of 2 □g/kg each, comprising only 10%-45% of the standard regimen. Experimental results of platelet formation (middle panel) and MPV measurements (lower panel) following conventional rmTPO therapy (black diamonds) and the alternative therapy (white squares) in mice, according to the above schedules, validate the model predictions. Treatments are initiated at day 0. Average ± s.d. of five mice are shown, per each entry (data adapted from [38efs. 37 and 38.)

were experimentally applied to mice clustered in two experimental arms, and their subsequent responses were compared. Mice of the first arm (A) received a standard regimen consisting of a single injection of 17.5 μg/kg recombinant murine TPO (rmTPO), which was well below the reported saturating level [42]. The second arm (B) tested the model-generated proposition that the same platelet yields can be obtained in mice receiving a total dose of 8 μg/kg rmTPO, divided over four equal daily injections, whereas the null hypothesis here was that a significantly smaller total dose of rmTPO would be less efficient in elevating the platelet counts.

The results of the experiments, presented in figure 36.6 (middle panel), clearly show that the platelet profile of arm A (a regimen of one 17.5 μg/kg rmTPO injection), is similar to the profile of arm B (applying a regimen of four daily 2μg/kg rmTPO doses). The differences are statistically insignificant, as evaluated by the student's t-test. The average profiles of both arm A and B peaked at fairly the same time (day 5 vs. day 6, respectively) and at similar mean platelet counts of 2741±193 x 109/L and 2685±164 x 109/L, respectively. The latter schedule resulted in a slightly extended thrombocytosis. MPV, known to decrease in platelet production induced by low dose TPO in mice [55], was compared between arm A and arm B as well (figure 36.6, lower panel). Results show that the familiar phenomenon of MPV reduction also occurred similarly in both groups. Once again, arm A had preceded arm B in reaching its nadir by about 24 hours (6.76 fL on day 6, vs. 6.74fL on day 7, respectively). Specific adverse effects were not observed following either treatment.

In order to evaluate in Rhesus monkeys the efficacy of the treatment regimen, already validated in mice, we first checked the ability of the simian thrombopoiesis model to predict individual monkey responses to different TPO treatments. Next, the simian response to the model-suggested schedule was simulated and the resulting predictions were compared with the platelet counts that were experimentally obtained under the model suggested schedule.

To this end, model parameters were first evaluated to fit the empirical platelet profile of a single Rhesus monkey. The quantitatively adequate simulations of thrombopoiesis response to treatment were apparent from their resemblance to the empirical results (figure 36.7). This calibrated model was further validated in several other monkeys, each receiving a different drug schedule (see schedule in figure 36.8, top panel).

Results in figure 36.9 demonstrate that the model predictions run remarkably close to the empirical data points. Note that as the platelet counts were monitored in these monkeys only once weekly, a mismatch is introduced into the comparison between the empirical results and the daily predicted counts. Therefore, there is no reason to assume that the peaks in the predicted responses on days that were not tested empirically, did not actually take place.

36.5.3 Predicting the optimal TPO toxicity/efficacy ratio in monkeys

Once verified, the Virtual Rhesus model was simulated for identifying an improved TPO administration regimen. The model-based regimen was then evaluated for verifying its improved efficacy and safety profile. This was done in two monkeys (see figure 36.8, bottom panel). The resulting elevation in platelet counts peaked at 1700

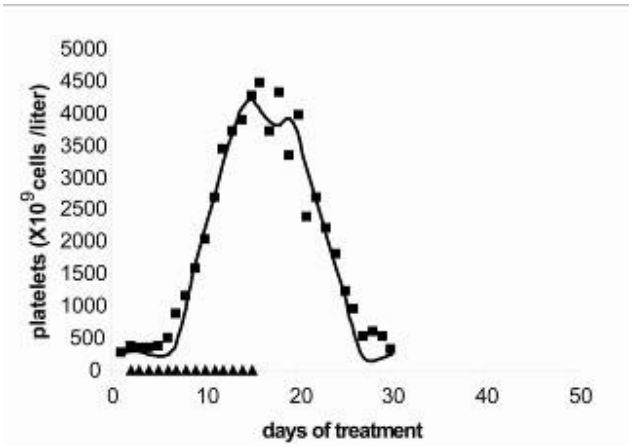

FIGURE 36.7: Comparison of model predictions to empirical data of TPO therapy in a Rhesus monkey. Daily experimental measurements (rectangles) are shown as well as model simulations (solid line) of platelet counts of one monkey treated by TPO. Fourteen daily doses of 5 μg/kg TPO were applied, administration days marked by triangles (data adapted from [37 and 38]).

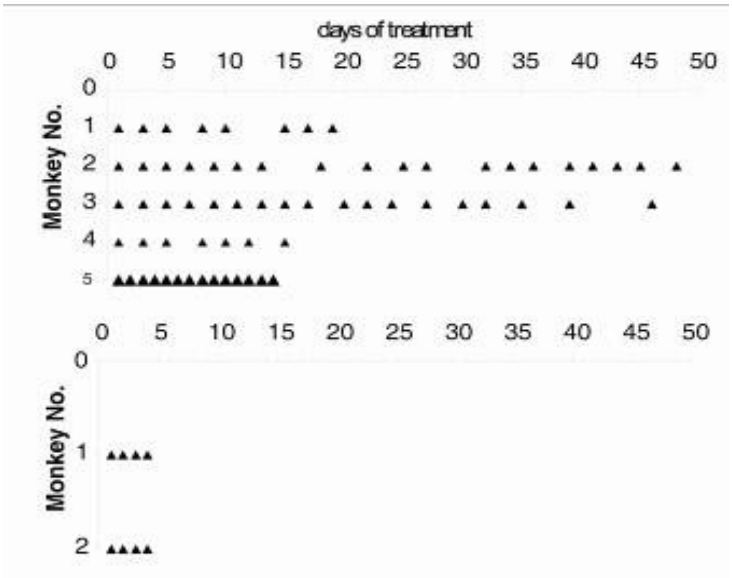

FIGURE 36.8 TPO administration schedules applied in simians for model validation. Upper panel: Five different schedules, comprising various combinations of 5 μg/kg doses of recombinant full length Rhesus monkey TPO (each dose indicated by triangles), were individually applied to the studied monkeys. Lower panel: model-suggested TPO schedules (also using doses of 5 μg/kg) applied to two monkeys.

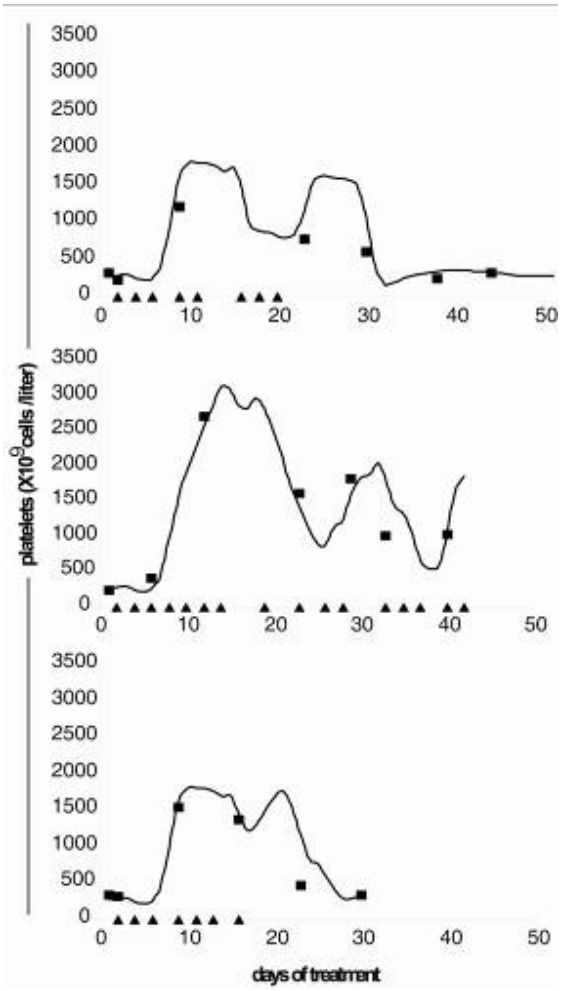

FIGURE 36.9 Comparison of model predictions to experimental platelet profiles of Rhesus monkeys under various TPO treatment schedules. Three monkeys (upper, middle, and lower panels) were subjected to individual TPO regimens, consisting of multiple dosing treatments of 5 μg/kg TPO, administration days marked by triangles. Experimental measurements of platelet counts in blood were performed weekly or bi-weekly (squares), and are plotted against model simulations (solid line).

- 2400x109/L following each treatment cycle. The results of a second cycle of the same treatment were similar to those of the first one in showing no neutralizing Antibodies. Only when the dosing cycle was applied for the third time, low antibody titers were detectable, which did not jeopardize TPO's efficacy and did not result in decreased platelet counts. The individual empirical responses of the two monkeys to the first treatment cycle are shown in figure 36.10, top panel (to be compared with a highly immunogenic response of a monkey who underwent another TPO treatment, figure 36.9, bottom panel).

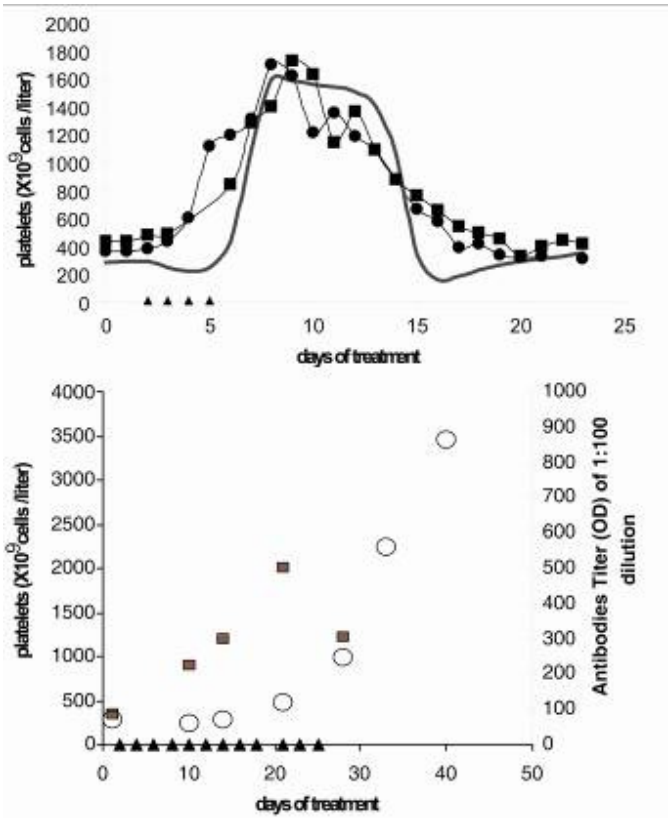

FIGURE 10 Superiority of the model-suggested TPO treatment schedule validated in Rhesus monkeys, as compared to other regimens. Upper panel: empirical platelet profiles of monkeys under the model-suggested TPO regimen of 4 daily 5 μg/kg doses (solid squares and circles) are plotted, administration days are marked by triangles. Lower panel: Antibody titer and platelet profiles of a monkey undergoing an arbitrary treatment by 12 TPO doses.

These results show that the model predicted administration regimen of smaller TPO doses with an interval of 24 hours yields platelet counts that are equal in effect to the more than double dose regimen, administered as a bolus injection. This experiment joins previous in vivo experiments with other drugs in verifying a mathematical theory discussed in section 36.1.1, which essentially suggests that treatment efficacy can be decisively influenced by modulating the inter-dosing interval according to the internal cell kinetics. The monkey experiment supports the model prediction of an equally efficient and non-immunogenic treatment, if dose is fractionated by an appropriate dosing-interval. Importantly, this schedule, adopted for improving safety of TPO administered for platelet harvesting in monkeys, has been in use for the last five years, or so. No adverse effects have been associated with this model-suggested treatment.

In general terms, the experimental results in both animal species supported and validated the predictions of the mathematical model that more efficacious treatment with TPO can be implemented. Although, intuitively it may not seem beneficial for

the patient to replace a single injection by multiple doses, it is clearly of significance for safety considerations.

The computerized mathematical model is capable of successfully predicting treatment scenarios not yet tested experimentally, as well as of identifying safer regimens. This tool is expected to be of aid in suggesting improved drug strategies for an individual or for a patient-population. Human trials are necessary for testing the suggested improved TPO strategies, possibly in conjunction with chemotherapy.

36.6 Using the thrombopoiesis model for predicting an unknown animal toxicity mechanism

Several pathophysiological mechanisms can account for drug-induced TP (see section 36.3), and the actual underlying mechanism in each particular case can have important therapeutic implications. Yet, no easily applicable non-invasive laboratory tests are available for distinguishing between the different mechanisms for TP. In this section, we describe the manner by which mathematical modeling can help understand dynamics and etiology of drug-induced TP.

A monoclonal antibody-based drug, developed against a platelet-unrelated antigen and currently under preclinical evaluation, was found to possess cross-reactive effects eliciting severe TP in monkeys. Despite routine laboratory testing and histological examination of bone marrow of affected monkeys, the drug's mechanism for inducing TP has not been elucidated. In an attempt to decipher the underlying mechanism, we used the mathematical model for TPO-regulated thrombopoiesis [37,38], which was previously formed (as described in section 2) and validated in vivo (as depicted in sections 36.4 and 36.5). This model was extended to include the effect of the drug on MKs and platelets. Since the mechanism is still unknown, several biologically-plausible alternatives were examined. Antibodies can exert their effect either by antibody-assisted phagocytosis, or by complement-mediated direct toxicity [56]. In the first mechanism, antibody-covered platelets or platelet-forming MKs would be efficiently removed by macrophages that bear specific antibody-recognizing receptors. In the latter case, platelet-bound antibodies activate the complement pathway that leads to cell membrane perforation and cell destruction (figure 36.11). Mathematical implementation of both antibody-mediated killing mechanisms into the PD-extended model was performed as follows. For complement-mediated toxicity, an “accumulated hits” model, according to which each platelet suffers from cumulative damage (“hits”) induced by antibody-mediated complement binding, was suggested. Upon accumulation of a certain number of “hits”, the platelet is permanently damaged. The resulting probability density function, P(t), describing a fraction of platelets with a given number of “hits” in time t post-exposure, is given by the gamma function

$$P(t) = \frac{(\alpha t)^m e^{-\alpha t} \alpha}{m!},$$

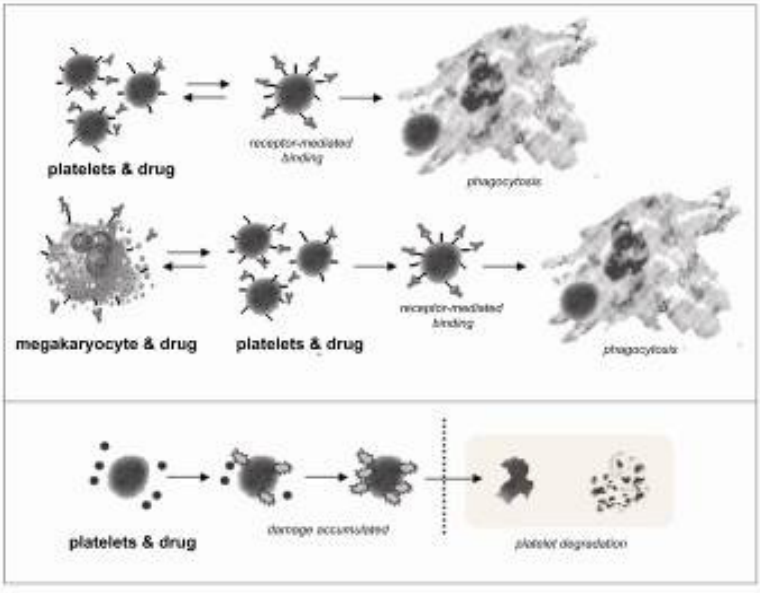

FIGURE 36.11 The “phagocytosis” putative mechanism and the "hits" putative mechanism of drug-induced thrombocytopenia. In the “phagocytosis” mechanism (upper panel), drug molecules bind to platelet and megakaryocyte surface antigens, leading to their phagocytosis by the reticuloendothelial system. In the "hits" mechanism (lower panel), drug molecules bind to platelet surface antigens, leading to complement activation and direct destruction of the cells.

where m is the number of “hits” needed for platelet destruction, and α is the rate of “hit” formation. The rate of “hits” is given by a linear function of the antibody concentration in blood:

$$\alpha = aX + b,$$

where X is antibody concentration , and a and b are parameters.

For the case of antibody-mediated phagocytosis, the "phagocytosis" model, it was assumed that the rate of platelet “capture” by macrophages has a form of Hill's function, depending on the number of antibodies that are bound to the platelets surface. This is described, as follows

$$B(i) = \frac{B_{\max} * i^z}{K^z + i^z},$$

where B(i) is the rate of capture of platelets that possess i bound antibodies, and K and z are parameters. Since binding and dissociation of antibodies from the platelet surface are stochastic processes, the distribution of platelets with respect to the number of bound antibodies, Vi, was explicitly calculated, so that the rate of antibody-induced platelet elimination is given by

$$R = \sum_i V_i * B_i .$$

Antibodies can act against mature platelets, bone marrow-derived MKs, or both. Hence, several combinations of these suggested drug-toxicity mechanisms were implemented in the extended model. Retrospective results of real-life experiments

in a number of individual Rhesus monkeys [37,38] were used for comparison with the simulated outcomes of these various alternative models. For each combination, the PD-associated parameters of the extended model were adjusted to best fit to these experimental results. Only one of the combinations was expected to consistently retrieve experimental data, and thus be identified as the preferable mechanism underlying this antibody-mediated TP. Systemic platelet profiles in individual monkeys following administration of multiple or single doses of the drug were compared with the best-fit profiles produced by models with different drug effect mechanisms (figure 36.12). The analysis of these simulations indicated that the "hits" model failed to predict dynamics of the drug-induced TP, while the "phagocytosis" model coincided with experimental data. Model results also show that by assuming toxicity to both platelets and MKs, rather than to just platelets, more precise predictions can be yielded.

We conclude that the developed computerized thrombopoiesis model superimposed by mathematical models for putative toxicity mechanisms can retrieve adverse thrombocytopenic effects recorded empirically in simians. Different models of drug toxicity mechanisms yield different profiles of blood platelets, yet the antibody-mediated phagocytosis of platelets and MKs seems the most plausible mechanism of the drug-induced TP in this situation. In this manner, mathematical modeling can help decipher the underlying mechanisms of other disorders.

36.7 Transition to Phase I

Drug development is a costly and time-consuming endeavor, due to its requirement for enormous collections of data concerning the efficacy and safety of the proposed drug. The ability to extrapolate toxicity and efficacy data from animal to human is therefore of great importance for efficiently advancing development of pharmaceuticals. Yet, despite the efforts invested in this direction, and the great advances achieved in recent years, extrapolation of data from animals to humans is still considered unreliable [57-59]. In this section, we provide a detailed description of an algorithm, which in conjunction with data from cell cultures and animal experiments, can be used for the modeling of clinically-stimulated (drug-induced) TP in humans, and show how this method enables good clinical predictability of this disorder.

As discussed in section 36.3, TP can result from therapeutic intervention, such as anticancer chemotherapy. The mathematical model of thrombopoiesis, described in section 36.2, was used as a basic model for retrieving clinical cytotoxic drug-

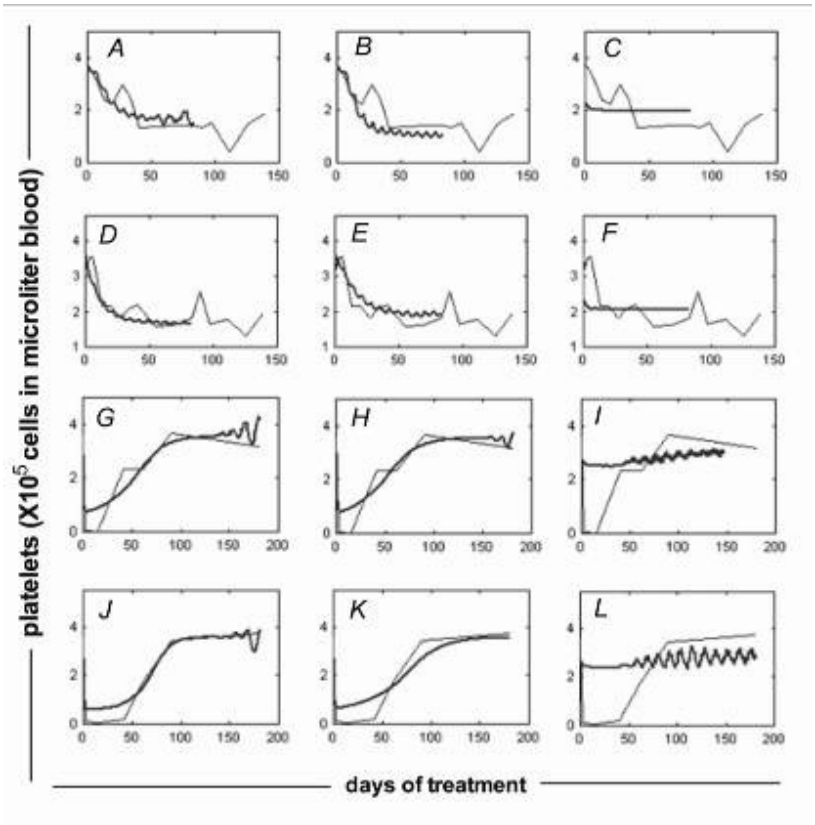

FIGURE 36.12 Model retrieval of drug-induced thrombocytopenia in Rhesus monkeys. Platelet dynamics derived from experiments in four monkeys, receiving a treatment of multiple doses (A-F) or a single high dose (G-L) of the drug. The effects of each treatment on the monkey's platelet profile were simulated by the three mathematical models of alternative drug-toxicity mechanisms. Model predictions were then statistically compared with the experimental results. Simulation results of the "phagocytosis" model assuming that the drug targets platelets alone (left column panels), of the "phagocytosis" model assuming that the drug targets both platelets and megakaryocytes (middle column panels), or of the "hits" model, assuming that the drug targets only platelets (right column panels). Panels A-C, D-F, G-I and J-L correspond to data from each of the four monkeys. Empirical data (thin lines) is shown vs. simulation-derived dynamics (thick lines).

induced TP. Yet, to obtain a reasonable approximation of the predicted toxicity in humans, based on preclinical data, additional assumptions and simplifications are required. These are detailed below.

First, translation of drug PD from the preclinical to the clinical stage is necessary. One must consider (a) differences between in vitro and in vivo data, and (b) differences between PD parameters of different species. Both variation types involve built-in inaccuracies: With respect to the comparison between in *vitro* and *in vivo* experiments, a few issues must be taken into account. Cells *in vitro* are more sensitive to a drug, and thus more susceptible to drug-induced apoptosis. They have higher mitotic indices due to less contact inhibition, and are usually exposed to constant levels of drug concentration over time. Cells in the physiological, whole-organism context, however, are of lower sensitivity to a drug; the surrounding microenvironment, consisting of high proliferating and less drug-susceptible cells,

provides a constant influx of healthy cells into the total pool, thereby limiting the damage caused by the drug [60]. Differences in exposure to growth factors between the two experimental settings exist as well. Drug sensitivity differs not only between *in vitro* and *in vivo* settings, but also in various species, which may differ in size of cells, mitotic indices of various compartments and differential stages of cells, apoptotic indices, transit times, sensitivity to hormones, etc. [61].

In order to replicate clinical use of the drug, the basic mathematical model iss extended to incorporate an additional formula for the drug PD. It is assumed that bone marrow cells are exposed to systemic drug concentration at any time, as the tissue is highly vascularized. The model also assumes that cells at different developmental stages, denoted by a subscript X (e.g. UCP, CP, EP), are of diverse sensitivity to the drug. The functional relation between the concentration of the cytotoxic drug in blood (CDbl) and the cytotoxic effect (CE) is given by the equation

$$CE_x(t) = f\left(CD_{bl}(t)\right), \qquad (36.14)$$

where CEx denotes the fraction of bone marrow thrombopoietic cells of a differentiation stage X, eliminated following exposure to CDbl at time t (CDbl(t)). The dependence is represented by function f, where $0 \le f\left(CD_{bl}(t)\right) \le 1$ for any t.

Most cytotoxic drugs target mitotic phases of the cell cycle, and are thereby more harmful to proliferating, rather than resting, cells. Accordingly, by further subdividing the model compartments into cell-cycle phases (G0-G1 and S-G2-M sub-compartments), a more accurate prediction of drug toxicity can be obtained. For example, in the above model, representation of UCP and CP compartments (see section 2) uses cell-cycle length instead of amplification rate. This allows us to calculate, not only the total number of cells remaining at every time point after drug application, but also the number of cells at every age and cell-cycle phase. In EP compartments, the age and the position in the endomitotic cycle are synchronized, thus there is no need for additional distribution. The rest of the compartments, consisting of non-dividing cells, are not considered susceptible to the standard cytotoxic drug, and are therefore not subdivided in this manner. Cytotoxic drugs that selectively target these stages can be addressed after subdivision of those compartments. In this complex form of the model, parameters (e.g. compartments sizes, transit times), are evaluated differently for all the species examined, while the model equations themselves remain of the same structure.

Following adaptation of the model equations to include the PD of the drug, parameters are calibrated using the available experimental information. Preclinical toxicity data to be used by the model consist of the platelet measurements over time in one animal of a chosen species (S), which has shown (in previous in vitro studies) higher sensitivity to the drug than other species. Various sets of data are obtained for a wide range of drug doses, so that different thrombocytopenic responses, from low toxicity to grade 3-4 toxicities, are considered.

The model also exploits data from cell culture assays. For example, for the estimation of the cytotoxic drug concentration, the model uses IC20, IC50 and IC90 (the concentrations of the drug leading to inhibition of 20%, 50%, and 90% of in vitro cell growth, respectively, as compared to untreated cells), These are obtained from toxicity tests of the platelet lineage-committed bone marrow cells (the CFU-Meg assay), in both human and species S-derived cells [62]. In the complex form of the model, one may also use experimental tools of cell cycle analysis, such as standard cell-sorting assays.

Based on this data, three functions f (Eq. 36.14), denoted as finVitroHu, finVitroS, and finVivoS for human cell cultures, species S cell cultures, and preclinical S species studies respectively, can be evaluated. In estimating the function finVivoS, it is necessary to consider only the drug's killing effect on bone marrow cells of compartment X, the depletion of which is mainly responsible for platelet nadir (see Eq. 36.14). X is identified by the time of the nadir after drug application, taking into account the transit times of the different bone marrow compartments. As a first approximation, only one compartment X of drug-sensitive cells is assumed.

The parameters of function f in the clinical scenario (finVivoHu), which cannot be estimated as in the other three cases due to lack of data, are thereby calculated according to their counterparts: First, it is assumed that between different species, there is a linear relation between the drug killing effect observed in vivo and in vitro (that is, the finVivo /finVitro ratio is constant between diverse species). The function finVivoHu is thereby obtained by shifting the IC values on the concentration axis according to this relation, using the in vitro data of IC50 (IC50inVitroHu) and IC90 (IC90inVitroHu). The relation itself is found by comparing the in vitro and in vivo data for species S. Then the shift of finVivoS to finVivoHu on the concentration axis for IC50 is computed by the equation

$$IC50_{inVivoHu} = \frac{IC50_{inVivoS} \cdot IC50_{inVitroHu}}{IC50_{inVitroS}} \qquad (36.15).$$

The same method can be applied for IC90.

The last step requires simulations of the model with the human parameters, under different regimens, applying the finVivoHu effect on the same type of bone marrow cells as in species S. The clinical toxicity profile of the drug, that is, the induction and severity of drug-induced TP in humans, is therefore predictable. Importantly, though, this estimation is a first approximation and a safety factor should be considered prior to initiation of clinical trials.

36.8 Conclusion

- Mathematical models are instrumental in increasing the understanding of intricate drug-patient interactions. Specifically, a mathematically-based method, termed Z-method, has been devised for increasing efficacy/toxicity ratio of chemotherapeutics. The method suggests that safety of cell-cycle-specific drugs can be increased by resonating drug-pulsing with the internal periodicity of target host cells replication. Experimental verification of the Z-method in mice provides a proof-of-concept for the utility of biomathematics in drug development.
- Increasing model complexity, a prerequisite for the quantitative precision of its conclusions, was performed, in the aim of providing a practical tool for predicting drug effects on platelet counts. To this end, thrombopoiesis models of various mammal species have been developed. Models of TPO supportive treatment have been prospectively validated in mice and monkeys.
- Toxicity effects of IL-11 therapy and chemotherapy have been modeled and various drug regimens were tested. Model validation under data limitation has been examined and the need to collect patient’s recovery data has been emphasized. The range of the treatment schedules under which the models could reliably predict the outcomes of drug therapy under obscured biological knowledge has been defined.

- The thrombopoiesis model has been employed for suggesting TPO administration schedules, which would maximize drug safety while maintaining its efficacy. Dose fractionation, having a well-calculated, species-dependent dosing interval, preserves drug effect on platelet counts, yet reduces its immunologic adverse effects below the clinically relevant threshold.
- The above schedule, adjusted by the murine thrombopoiesis model, was validated in mice for efficacy. The monkey-adjusted schedule derived from simulations of the simian thrombopoiesis model, was validated in Rhesus monkeys for both efficacy and toxicity. Now the human model may be employed for improving safety of TPO mimetics and other thrombocytopenia alleviating drugs.
- To the best of our knowledge this is the first instance of a mathematical model generating quantitative predictions, the precision of which was validated in the preclinical setting.
- The thrombopoiesis model can be used, in conjunction with alternative mathematical models, for deciphering unknown drug toxicity mechanisms in different species. This can be achieved by comparing preclinical study results with the simulated drug-affected platelet profiles, generated for different models of putative drug toxicity mechanisms.
- In order to facilitate the transition from preclinical studies to Phase I, the mathematical models for the effect of investigational drugs on different animal species can be adapted accordingly and simulated in the human patient model for predicting parameters, the early estimation of which can economize Phase I clinical trials.

References

1. Agur, Z. (1982). Persistence in uncertain environments. Population Biology, Lecture Notes in Biomathematics (eds. Freedman, H.I., Strobeck, C.) Heidelberg, Springer-Verlag, 125-132.
2. Agur, Z. (1985). Randomness, synchrony and population persistence. *Journal of Theoretical Biology, 112,* 677-693.
3. Agur, Z., Deneubourg, JL. (1985). The effect of environmental disturbances on the dynamics of marine intertidal populations. *Theoretical Population Biology, 27 (1),* 75-90.
4. Agur, Z. (1986). The effect of drug schedule on responsiveness to chemotherapy. Annals of the New York Academy of Sciences, 504, 274-277.
5. Agur, Z. (1988). Population dynamics in harshly varying environments; evolutionary, ecological and medical aspects. Chapter in: Mathematical Ecology (Hallam T.G., Gross, L.J., Levin, S.A., eds.) *World Scientific*, 440-454.
6. Agur, Z., Arnon, R., Schechter, B. (1988). Reduction of cytotoxicity to normal tissues by new regimes of cell-cycle phase-specific drugs. *Mathematical Biosciences, 92,* 1-15.
7. Agur, Z., Arnon, R., Sandak, B., Schechter, B. (1991). Zidovudine toxicity to murine bone marrow may be affected by the exact frequency of drug administration. *Experimental Hematology, 19,* 364-368.
8. Agur, Z., Arnon, R., Sandak, B., Schechter, B. (1992). The effect of the dosing interval on myelotoxicity and survival in mice treated by cytarabine. *European Journal of Cancer, 28A (6/7),* 1085-1090.
9. Agur, Z. (1998). Resonance and anti-resonance in the design of chemotherapeutic protocols. *Journal of Theoretical Biology*, *1*, 237-245.

10. Agur, Z., Ziv, I., Shohat, R., Wick, M., Webb, C., Hankins, D., Arakelyan, L., Sidransky, D. Using a novel computer technology for tailoring targeted and chemotherapeutic drug schedules to the individual patient. *First AACR International Conference on Molecular Diagnostic in Cancer Therapeutic Development. Chicago IL, USA,* (2006).
11. Al-Dabbagh, S.G., Smith, R.L. (1984) Species differences in oxidative drug metabolism: some basic considerations. *Archives of Toxicology, Suppl. 7*, 219-31.
12. Arakelyan, L., Vainstein, V., Agur, Z. (2002). A computer algorithm describing the process of vessel formation and maturation, and its use for predicting the effects of anti-angiogenic and anti-maturation therapy on vascular tumor growth. *Journal of Angiogenesis, 5,* 203-214.
13. Arnold, J.T., Daw, N.C., Stenberg, P.E., Jayawardene, D., Srivastava, D.K., Jackson, C.W. (1997). A single injection of pegylated murine megakaryocyte growth and development factor (MGDF) into mice is sufficient to produce a profound stimulation of megakaryocyte frequency, size, and ploidization. *Blood, 89*, 823-833.
14. Basser, R. (2002). The impact of thrombopoietin on clinical practice. *Current Pharmaceutical Design, 8(5),* 369-77.
15. Castiglione, F., Selitser, V., Agur, Z. (2003). The analyzing hypersensitive to chemotherapy in a cellular automata model of the immune system. *Chapter in: Cancer Modelling and Simulation (Preziosi L. ed.), CRC Press, LLC, UK.*
16. Cines, D.B., Bussel, J.B., McMillan, R.B., Zehnder, J.L. Congenital and acquired thrombocytopenia. (2004). *Hematology, the American Society of Hematology Education Program Book*, 390-406.
17. Cojocaru, L., Agur, Z. (1992). A theoretical analysis of interval drug dosing for cell-cycle-phase-specific drugs. *Mathematical Biosciences, 109*, 85-97.
18. De Serres, M., Yeager, R.L., Dillberger, J.E., Lalonde, G., Gardner, G.H., Rubens, C.A., Simkins, A.H., Sailstad, J.M., McNulty, M.J., Woolley, J.L. (1999). Pharmacokinetics and hematological effects of the pegylated thrombopoietin peptide mimetic GW395058 in rats and monkeys after intravenous or subcutaneous administration. *Stem Cells, 17,* 316-326.
19. Demetri, G.D. (2001). Targeted approaches for the treatment of thrombocytopenia*. The Oncologist, 6 (Suppl. 5),* 15–23.
20. Dykstra, K.H., Rogge, H., Stone, A., Loewy, J., Keith, J.C. Jr., Schwertschlag, U.S. (2000). Mechanism and amelioration of recombinant human interleukin-11 (rhIL-11)-induced anemia in healthy subjects. *Journal of Clinical Pharmacology, 40(8),* 880-8.
21. Ebbe, S., Stohlman, F. (1965). Megakaryocytopoiesis in the rat. Blood, 26, 20-35.
22. Elting, L.S., Rubenstein, E.B., Martin, C.G., Kurtin, D., Rodriguez, S., Laiho, E., Kanesan, K., Cantor, S.B., Benjamin, R.S. (2001). Incidence, cost, and outcomes of bleeding and chemotherapy dose modification among solid tumor patients with chemotherapy-induced thrombocytopenia. *Journal of Clinical Oncology, 19,* 1137–1146.
23. Farese, A.M., Hunt, P., Boone, T., MacVittie, T.J. (1995). Recombinant human megakaryocyte growth and development factor stimulates thrombopoiesis in normal nonhuman primates. *Blood, 86,* 54-59.
24. FDA White Paper on Innovation and Stagnation in drug industry, Challenges and Opportunities on the Clinical Paths to New Medical Products, March 2004.
25. Harker, L.A., Finch, C.A. (1969). Thrombokinetics in man. *Journal of Clinical Investigation, 48*, 963-974.
26. Harker, L.A., Hunt, P., Marzec, U.M., Kelly, A.B., Tomer, A., Hanson, S.R., Stead, R.B. (1996a). Regulation of platelet production and function by megakaryocyte growth and development factor in nonhuman primates. *Blood, 87,* 1833-1844.
27. Harker, L.A., Marzec, U.M., Hunt, P., Kelly, A.B., Tomer, A., Cheung, E., Hanson, S.R., Stead, R.B. (1996b). Dose-response effects of pegylated human

megakaryocyte growth and development factor of platelet production and function in nonhuman primates. *Blood, 88,* 511-521.

28. Haznedaroglu, I.C., Goker, H., Turgut, M., Buyukasik, Y., Benekli, M. (2002). Thrombopoietin as a drug: biologic expectations, clinical realities, and future directions. *Clinical and Applied Thrombosis/Hemostasis, 8,* 193–212.
29. Hoffman, R., Benz, E.J., Shattil, S.J., Furie, B., Cohen, H.J., Silberstein, L.E., McGlave, P. *Hematology 3rd ed., Churchill Livingstone, 2000.*
30. Janeway, C.A., Travers, P., Walport, M., Shlomchik, M. Immunobiology. 6th ed. *New York: Garland Science, 2005.*
31. Kabaya, K., Akahori, H., Shibuya, K., Nitta, Y., Ida, M., Kusaka, M., Kato, T., Miyazaki, H. (1996). *In vivo* effects of pegylated recombinant human megakaryocytes growth and development factor on hematopoiesis in normal mice. *Stem Cells, 14,* 651-660.
32. Kararli, T.T. (1995). Comparison of the gastrointestinal anatomy, physiology, and biochemistry of humans and commonly used laboratory animals. *Biopharmaceutics and Drug Disposition, 16(5),* 351-80.
33. Kaushansky, K., Lin, N., Grossman, A., Humes, J., Sprugel, K.H., Broudy, V.C. (1996). Thrombopoietin expands erythroid, granulocyte-macrophage, and megakaryocytic progenitor cells in normal and myelosuppressed mice. *Experimental Hematology, 24,* 265-269.
34. Kaushansky, K. (2005). The molecular mechanisms that control thrombopoiesis. *Journal of Clinical Investigation, 115,* 3339–3347.
35. Kaushansky, K. (2006). Lineage-specific hematopoietic growth factors. *New England Journal of Medicine, 354,* 2034-45.
36. Kheifetz, Y., Elishmereni, M., Horowitz, S., Agur, Z. (2006). Fluid-retention side-effects of the chemotherapy-supportive treatment Interleukin-11: Mathematical modelling as affected by data availability. *Computational and Mathematical Methods in Medicine, in press.*
37. Kheifetz, Y., Kogan, Y., Agur, Z. (2006). Long-range predictability in models of cell populations subjected to phase-specific drugs: Growth-rate approximation using properties of positive compact operators. *Mathematical Models and Methods in the Applied Sciences, 16 (7),* 1-18.
38. Li, J., Yang, C., Xia, Y., Bertino, A, Glaspy, J., Roberts, M., Kuter, D.J. (2001). Thrombocytopenia caused by the development of antibodies to thrombopoietin. *Blood, 98(12),* 3241-8
39. Lin, J.H. (1995). Species similarities and differences in pharmacokinetics. *Drug Metabolism and Disposition, 23(10),* 1008-21.
40. Luoh, S., Stephanich, E., Solar, G., Steinmetz, H., Lipari, T., Pestina, T.I., Jackson, C.W., de Sauvage, F.J. (2000). Role of the distal half of the c-Mpl intracellular domain in control of platelet production by thrombopoietin *in vivo*. Molecular and Cellular Biology, 20, 507-515.
41. McCrae, K.R. Bussel, J.B., Mannucci, P.M., Cines, D.B. Platelets: an update on diagnosis and management of thrombocytopenic disorders. (2001). *Hematology, the American Society of Hematology Education Program Book*, 282-305.
42. Neelis, K.J., Hartong, S.C., Egeland, T., Thomas, G.R., Eaton, D.L., Wagemaker, G. (1997a). The efficacy of single-dose administration of thrombopoietin with coadministration of either granulocyte/macrophage or granulocyte colony-stimulating factor in myelosuppressed Rhesus monkeys. *Blood, 90,* 2565-2573.
43. Phillips, R. M., Bibby, M. C., Double, J. A. (1990). A critical appraisal of the predictive value of *in vitro* chemosensitivity assays. *Journal of the National Cancer Institute, 82,* 1457-1468.
44. Ratajczak, J., Machalinski, B., Samuel, A., Pertusini, E., Majka, M., Czajka, R., Ratajczak, M.Z. (1998). A novel serum free system for cloning human megakaryocytic progenitors (CFU-Meg). The role of thrombopoietin and other cytokines on bone marrow and cord blood CFU-Meg growth under serum free conditions. *Folia Histochemica et Cytobiologica, 36(2),* 61-6.

45. Ribba, B., Alarcon, T., Marron, K., Maini, P.K., Agur, Z. (2005). Doxorubicin treatment efficacy on non-Hodgkin's lymphoma: Computer model and simulations. *Bulletin of Mathematical Biology, 67,* 79-99.
46. Schermer, S. (1967). Blood morphology of laboratory animals. F.A. Davis Co., Philadelphia, PE.
47. Schulze, H., Shivdasani, R.A. (2005). Mechanisms of thrombopoiesis. *Journal of Thrombosis and Haemostasis, 3,* 1717–24.
48. Schwertschlag, U.S., Trepicchio, W.L., Dykstra, K.H., Keith, J.C., Turner, K.J., Dorner, A.J. (1999). Hematopoietic, immunomodulatory and epithelial effects of interleukin-11. *Leukemia, 13(9)*, 1307-15.
49. Siegers, M.P., Feinendegen, L.E., Lahiri, S.K., Cronkite, E.P. (1979). Relative number and proliferation kinetics of hemopoietic stem cells in the mouse. *Blood Cells, 5,* 211-236.
50. Skomorovski, K. Agur, Z. (2001). A new method for predicting and optimizing thrombopoietin (TPO) therapeutic protocols in thrombocytopenic patients and in platelet donors [abstract]. *The Hematology Journal, 1 (Suppl. 1),* 185.
51. Skomorovski K., Harpak H., Ianovski A., Vardi M., Visser TP., Hartong S., Van Vliet H., Wagemaker G., Agur Z. (2003). New TPO treatment schedules of increased safety and efficacy: pre clinical validation of a thrombopoiesis simulation model. *British Journal of Haematology, 123 (4),* 683-691.
52. Sola, M.C., Christensen, R.D., Hutson, A.D., Tarantal, A.F. (2000). Pharmacokinetics, pharmacodynamics, and safety of administering pegylated recombinant megakaryocyte growth and development factor to newborn Rhesus monkeys. *Pediatric Research, 47,* 208-214.
53. Tepler, I., Elias, L., Smith, J.W. 2nd, Hussein, M., Rosen, G., Chang, A.Y., Moore, J.O., Gordon, M.S., Kuca, B., Beach, K.J., Loewy, J.W., Garnick, M.B., Kaye, J.A. (1996). A randomized placebo-controlled trial of recombinant human interleukin-11 in cancer patients with severe thrombocytopenia due to chemotherapy. *Blood, 87(9)*, 3607-14.
54. Ubezio, P., Tagliabue, G., Schechter, B., Agur, Z. (1994). Increasing 1-beta-D-Arabinofuranosylcytosine efficacy by scheduled dosing interval based on direct measurement of bone marrow cell kinetics. *Cancer Research, 54,* 6446-6451.
55. Ulich, T.R., del Castillo, J., Senaldi, G., Cheung, E., Roskos, L., Young, J., Molineux, G., Guo, J., Schoemperlen, J., Munyakazi, L., Murphy-Filkins, R., Tarpley, J.E., Toombs, C.F., Kaufman, S., Yin, S., Nelson, A.G., Nichol, J.L., Sheridan, W.P. (1999). Megakaryocytopoiesis: The prolonged hematologic effects of a single injection of PEG-rHuMGDF in normal and thrombocytopenic mice. *Experimental Hematology, 27,* 117-130.
56. Vadhan-Raj, S., Murray, L.J., Bueso-Ramos, C., Patel, S., Reddy, S.P., Hoots, W.K., Johnston, T., Papadopolous, N.E., Hittelman, W.N., Johnston, D.A., Yang, T.A., Paton, V.E., Cohen, R.L., Hellmann, S.D., Benjamin, R.S., Broxmeyer, H.E. (1997). Stimulation of megakaryocyte and platelet production by a single dose of recombinant human thrombopoietin in patients with cancer. *Annals of Internal Medicine, 126,* 673-681.
57. Vadhan-Raj, S. (1998). Recombinant human TPO: clinical experience and *in vivo* biology. *Seminars in Hematology, 35,* 261–268.
58. Vadhan-Raj, S. (2000). Clinical experience with recombinant human thrombopoietin in chemotherapy-induced thrombocytopenia. *Seminars in Hematology, 37 (2 Suppl 4)*, 28-34.
59. Vadhan-Raj, S. (2001). Recombinant human thrombopoietin in myelosuppressive chemotherapy. *Oncology (Williston Park), 15 (7 Suppl 8),* 35-8.
60. Vadhan-Raj, S., Patel, S., Bueso-Ramos, C., Folloder, J., Papadopolous, N., Burgess, A., Broemeling, L.D., Broxmeyer, H.E., Benjamin, R.S. (2003). Importance of predosing of recombinant human thrombopoietin to reduce chemotherapy-induced early thrombocytopenia. *Journal of Clinical Oncology, 21,* 3158-3167.

61. Vadhan-Raj, S., Cohen, V., Bueso-Ramos, C. (2005). Thrombopoietic growth factors and cytokines. *Current Hematology Reports, 4(2),* 137-44.
62. Vainstein V., Ginosar, Y., Shoham, M., Ranmar, D., Ianovski, A., Agur, Z. (2005). The complex effect of granulocyte on human granulopoiesis analyzed by a new physiologically-based mathematical model. *Journal of Theoretical Biology, 234(3),* 311-27.
63. Vainstein, V., Ginosar, Y., Shoham, M., Ianovski, A., Rabinovich, A., Kogan, Y., Selitser, V., Ariad, S., Chan, S., Agur, Z. Clinical validation of a physiologically-based computer model of human granulopoiesis and its use for improving cancer therapy by doxorubicin and granulocyte colony-stimulating factor (G-CSF). *Annual Meeting American Society of Hematology (ASH), Orlando, FL, USA., 2006.*
64. Wagemaker, G., Hartong, S.C., Neelis, K.J., Egeland, T., Wognum, A.W. (1998). *In vivo* expansion of hemopoietic stem cells. *Stem Cells. 16 Suppl 1*, 185-191.
65. Wolff, S.N., Herzig, R., Lynch, J., Ericson, S.G., Greer, J.P., Stein, R., Goodman, S., Benyunes, M.C., Ashby, M., Jones, D.V. Jr, Fay, J. (2001). Recombinant human thrombopoietin (rhTPO) after autologous bone marrow transplantation: a phase I pharmacokinetic and pharmacodynamic study. *Bone Marrow Transplantion, 27(3),* 261-8.